S V E U Č I L I Š TE U S P L I T U
FAKULTET ELEKTROTEHNIKE, STROJARSTVA I BRODOGRADNJE

POSLIJEDIPLOMSKI DOKTORSKI STUDIJ ELEKTROTEHNIKE I INFORMACIJSKIH TEHNOLOGIJA

KVALIFIKACIJSKI ISPIT

POJEDNOSTAVLJENI ANALITIČKI MODELI ZA ODREĐIVANJE ELEKTROMAGNETSKO-TOPLINSKOG ODZIVA LJUDSKOG TIJELA IZLOŽENOG ZRAČENJU VISOKIH FREKVENCIJA

Enida Cero Dinarević

Split, Studeni 2023.

U N I V E RS I T Y OF S P L I T
FACULTY OF ELECTRICAL ENGINEERING, MECHANICAL ENGINEERING AND NAVAL ARCHITECTURE

POSTGRADUATE STUDY OF ELECTRICAL ENGINEERING AND INFORMATION TECHNOLOGY

QUALIFICATION EXAM

SIMPLIFIED ANALYTICAL MODELS FOR THE ASSESSMENT OF ELECTROMAGNETIC-THERMAL RESPONSE OF THE HUMAN BODY EXPOSED TO HIGH FREQUENCY RADIATION

Enida Cero Dinarević

Split, November 2023.

CONTENTS

1 Introduction

Due to the increasing use of mobile terminals, the importance of several aspects of interaction of electromagnetic (EM) waves with the human body has increased significantly. On the other hand, rapid technological development and the widespread presence of smart environments has led to the need for rapid implementation of systems, which further means rapid assessments of the impact of these systems on the human body.

Computer methods for analyzing problems in EM field generally fall into one of three categories: analytical techniques, numerical techniques, and expert systems [1]. Analytical techniques make simplifying assumptions about the geometry of a problem and EM field (EMF) equations are solved directly [1]. Numerical techniques attempt to solve fundamental field equations directly, subject to the boundary constraints posed by the geometry. Expert systems do not actually calculate the field directly, but instead estimate values for the parameters of interest based on a rules database [1].

All effects (thermal and other) of the exposure to EMFs must be well researched or described, regardless of whether one wants to protect himself from the potential harmful effects of EMF or to take advantage of their potential positive effects. The most important challenges regarding techniques for calculating EMF can be summarized as follows [2]:

- challenges related to the properties of biological tissue, which include magnetic permeability, electrical permittivity and electrical conductivity. The mentioned properties are not sufficiently well described and are dependent on a person's activity, because the material is active at the cellular level. These challenges are present in analytical and numerical techniques and expert systems.
- challenges associated with the coupling phenomena, since the dominant thermal effect is dependent on blood circulation. These challenges are present in analytical and numerical techniques and expert systems.
- challenges associated with the complex geometry of the problem that needs to take the environment into account. These challenges are partially addressed in analytical methods.

In the past few decades there has been a lot of effort to cope with the aforementioned challenges

keeping in mind computer resources and a minimum level of accuracy. Analytical methods offer a compromise between acceptable accuracy of said approach and saving computer resources.

Keeping what we said beforehand in mind, our goal is two-fold. At the beginning we highlighted the importance of the topic, so the Chapter 2 introduces some basic concepts of evolution of mobile network technologies (2G – 5G) and the main difference between different generations of mobile network.

In chapter 3 the interaction between human being and EMF is described. The basic potential risk associated with excessive exposure to EM radiation and some guidance for human health protection from the harmful effects of EM waves are given. The recommendations for exposure limitation are given in different frequency ranges, highlighting High Frequency (HF) range.

The second goal is to outline some of the commonly used analytical methods in electromagnetic-thermal dosimetry along with the advantages and limitations. Incident dosimetry concept are described in chapter 4. Different methods for dosimetry are explained and then short literature review of analytical approaches is given with the aim to emphasis possible simplification and advantages offer by these approaches to EM dosimetry. After detailed explanation of analytical methods, simple scenario with vertical Hertzian dipole antenna in far field is observed and corresponding field equations are presented.

After incident dosimetry concept, basic concepts of internal EM dosimetry are given in chapter 5. Since analytical methods are used when a problem requires an accurate solution, they are mostly related to canonical problems. Further on, comparison between canonical models and complex voxel models are given, followed by short description of basic canonical models mentioned in analyzed literature.

In chapter 6, thermal dosimetry concepts are explained followed by analytical approaches to solution of Penne's bioheat equation, as the most used equation for energy balance between conductive heat transfer per tissue volume unit, heat losses due to perfusion, metabolism and energy absorption due to radiation.

Finally, chapter 7 gives some conclusion remarks, pointing the problem towards the need for the spectrum of analytical methods that are accurate enough, but simple enough, to be used in the upcoming 5G systems and broader.

2 The history of mobile network

In past few years, mobile wireless communication has experienced different generations of technology, abbreviated to “G”, mainly from 2G to 5G (Figure 2.1.).

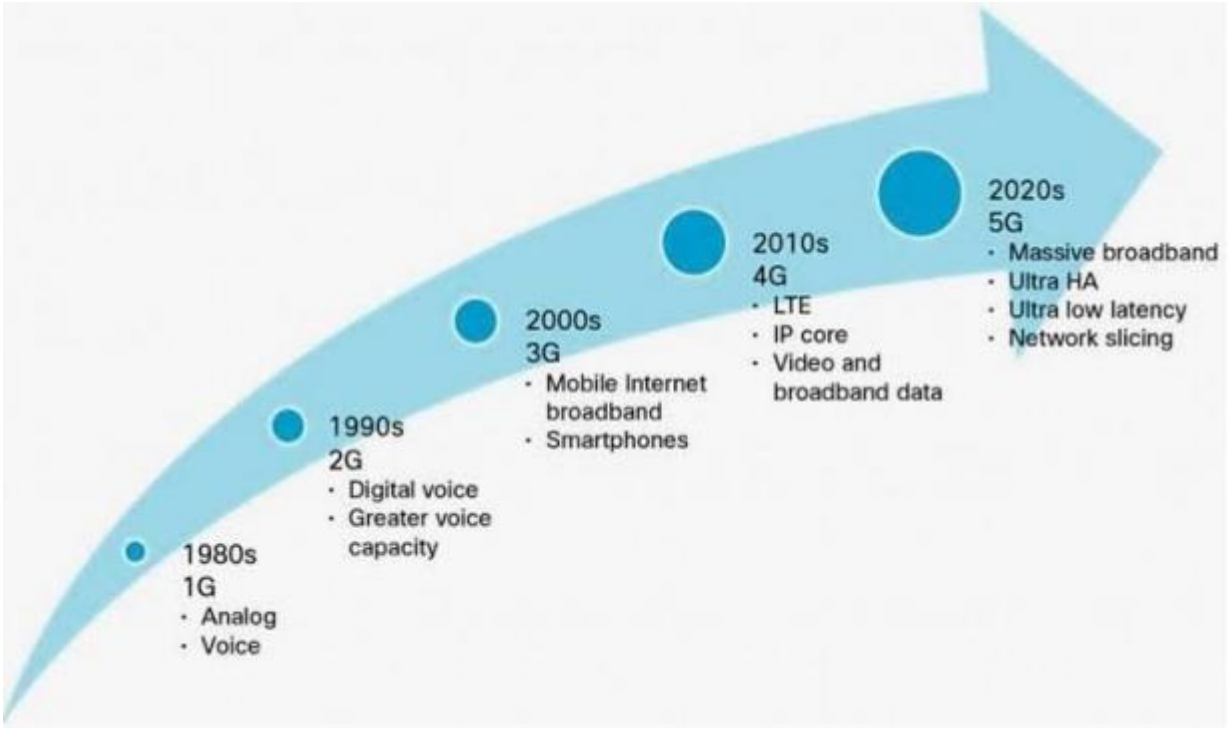

Figure 2.1. Evaluation of Wireless Mobile Generations [3]

Every successive generation of wireless standards have introduced advances in data-carrying capacity and decreases in latency. In the rest of the chapter, the basic characteristics of digital 2G - 5G mobile telephony, stating their basic advantages and disadvantages will be presented.

2.1 2G mobile networks

2G cellular network was introduced commercially in Finland in the year 1991 and launched on the Global System for Mobile communication (GSM) standard. 2G introduce various advantages of digital system over analogy system [4], such as improved sound quality, better security, able to cover up long distance, less prone to noise and more efficient [5]. 2G used digital signals for voice transmission, had a speed up to 64 kbps, and also provided the facility of Short Message Service (SMS) service [6].

Digital mobile access technology used in 2G are Time Division Multiple Access (TDMA) and Code Division Multiple Access (CDMA) [7], and in practice, the TDMA and CDMA schemes are combined with Frequency Division Multiple Access (FDMA) [8]. Today's GSM systems

work in the 900 MHz and 1800 MHz bands worldwide, except for the Americas where they operate on the 1900 MHz band [9]. Independent of the frequency band deployed, 124 traffic channels are provided for the uplink and downlink direction [10]. General Packet Radio Service (GPRS) is extension of existing 2G network, introduced in 1995 [10] which evolved later to Enhanced Data rates for GSM Evolution (EDGE). EDGE is the final step in the evolution of mobile telephony from 2G (GSM) to 3G [10]. The most important benefit of using EDGE technology is that one does not need to install any additional hardware and software on account of make use of EDGE technology [9].

Some key benefits of 2G network over its predecessors is better quality and capacity, consumes less battery [9], improves the voice clarity, reduces noise on the line, and gives security and safety to the data and voice calls [6]. The drawback of 2G is need for high level digital signals, and 2G is not adequate for web browsing and the other multimedia applications [9].

2.2 3G mobile networks

3G is the third generation of mobile phone standard and technology which provides high speed data transmissions of 144 kbps to 384 kbps in wide coverage areas and 2 Mbps in local coverage areas [9, 11]. 3G is based on International Mobile Telecommunications (IMT-2000) standard, defined by International Telecommunication Union (ITU), and later expanded by an organization called 3rd Generation Partnership Project (3GPP), called Universal Mobile Telecommunication System (UMTS) in Europe [11]. 3G uses Wideband Code Division Multiple Access (WCDMA).

In UMTS network, in contrast to the GSM standard, subscriber is physically connected with the network only as long as data is transferred, meaning data transmission in UMTS is packet switched [10]. The biggest difference between 2G and 3G systems is speed. 3G systems have enhanced audio and video streaming (faster data rates), support multimedia applications such as video and photography [7]. High Speed Packet Access (HSPA) is integration of High-Speed Downlink Packet Access (HSDPA) and High-Speed Uplink Packet Access (HSUPA). HSPA, also called 3.5G, provides data rate up to 14,4 Mbit/s (compared with 2 Mbps for WCDMA [12]) in downlink and 5,76 Mbit/s in uplink [7] and reduces latency from 180-200 ms to 100 ms [12].

3G technologies enable network operators to offer users a wider range of more advanced services while achieving greater network capacity through improved spectral efficiency [7, 9]. Basic disadvantages of 3G is that they require 3G compatible handsets, and the cost of upgrading to 3G devices is expensive [13]. Further on power consumption is high and 3G requires denser base stations which is expensive [13].

2.3 4G mobile networks

4G technology is an Internet Protocol (IP) based network system which offers a download speed of 1 Gbps (stationary user) and 500 Mbps in upload [9, 14] compared to 21 Mbps in downlink and 5 Mbps in uplink offered by 3G [14]. 4G provides additional services, mostly data and multimedia services with premium quality and high security [15]. High-definition mobile television, video on demand, video conferencing, IP telephony, gaming services, tele-medicine, location-based services, and 3D television are the applications supported in 4G cellular networks [4, 16].

4G is pure IP-based network system [4]. The first release of Long-Term Evolution (LTE) standard is designed to meet carrier needs for high-speed data and media transport as well as high-capacity voice supports [17]. Radio coding technology for the downlink is Orthogonal Frequency Division Multiple Access (OFDMA) and for uplink Single- carrier FDMA is a frequency division multiple access radio (SCFDMA) instead of WCDMA in UMTS [18].

Some advantages offer by 4G are [13] high spectral efficiency and high voice quality, easy access to internet services, streaming media, video calling, very low latency, simple protocol architecture, and efficient multicast/broadcast. Further on, the applications developed by 4G services are highly user friendly. Basic disadvantages of 4G [13] are higher data prices for consumers, and hard implementation with complex hardware for providers.

2.4 5G mobile networks

The need for higher transmission rates and higher overall network capacity (peak rate up to 20 Gbps) is a great motivator for new 5G technologies. 5G will meet constantly growing demands of mobile network users, as well as those imposed by innovative concepts, such as connected and autonomous cars, smart Factories or smart cities [19].

Among the most significant causes of the large increase in mobile data are (1) increased usage of mobile devices (e.g. smartphones, tablets, embedded Subscriber Identity Module (SIM) cards in laptops), (2) content availability and ubiquity in video streaming services providers (e.g. Netflix, YouTube) and (3) increased amount of user-generated content co-hosted on several social cloud platforms [20]. Since all requirement are hard to fulfill, requirements of the 5G-enabled service spectrum, are categorized as: (1) enhanced Mobile Broadband (eMBB), (2) ultra-Reliable and Low Latency (uRLLC), and (3) Massive Machine Type Communications (mMTC).

In order to fulfill the aforementioned requirements, it is expected that 5G systems will communicate at significantly higher frequencies compared to existing fourth generation systems or LTE systems. The frequency spectrum in the 5G network includes re-purposed frequency band below 6 GHz [21], and/or the mm-wave frequency spectrum (28 and 39 GHz) [22]. Lower spectrum enables fast data transfer, but over short distances due to line of sight propagation with minimal refraction. Small cells whose operating frequency is from 1 GHz to 6 GHz (and especially in the range from 3.3 GHz to 3.8 GHz) are especially suitable for meeting the conditions of coverage and capacity. The sub-6 GHz spectrum is very crowded, and already includes 3G/4G cellular, GPS, Wi-Fi, L-band satellite, S-band and C-band radars and other allocations. The 3.5 GHz frequency band was selected as the first band for 5G deployment and it is available in many countries around the world.

MM-wave spectrum is characterized by low efficient propagation over long distances, or attenuation of signals penetrating through obstacles such as glass windows or concrete walls. Ultra-high transmission speeds can be achieved in pico-cells with frequencies from 24 GHz to 28 GHz, but shifting the frequency from 70/80 to 60 GHz decreases the operating range from 3 km to 400 m [11, 20, 23].

Significant reduction in latency (no more than 1 ms), dramatic increase in the number of connected devices (device density up to one million per square kilometer), and reliable links (99.999%) with high coverage are just some of the requirements related to these systems. Further on, to meet the complex and sometimes contradictory requirements of diverse use cases, 5G ecosystem will encompass both a modernization of current 4G networks system and the addition of a new standards for access technology known as New Radio (NR) developed by 3GPP. This new radio enables effective use of the crowded and fragmented spectrum, a

simultaneous use of different Radio Access Technologies (RATs) and more flexibility of resource allocation. Innovative technologies such as the implementation of small cells (Ultra Dense Network (UDN)), Device-to-Device (D2D) communication, heterogeneous networks, and three-dimensional beamforming (3DBF) techniques [24] are just some of the proposals for implementation in fifth generation systems.

Summary of characteristics of different generation of mobile technologies are shown in Table 2.1.

Table 2.1 Characteristics of 2G – 5G mobile technologies

Technology/ Features	**2G**	**3G**	**4G**	**5G**
Start/deployment	1980-1999	1990-2002	2000-2010	2014
Location of first commercialization	Finland	Japan	South Korea	South Korea
Data bandwidth	64 Kbps	2 Mbps	1 Gbps	>1 Gbps
Frequency	800-1800 MHz	1.8-2.5 GHz	2-8 GHz	3-300 GHz
Technology	Digital Cellular Technology	CDMA 2000 UMTS, Edge	Worldwide Interoperability for Microwave Access (WiMax) LTE Wi-Fi	World Wide Web (WWW)
Service	Digital Voice, SMS, Higher capacity packetized data	Integrated high quality audio, video and data	Dynamic information access, wearable devices	Dynamic information access, wearable devices with AI capabilities
Multiplexing	TDMA, CDMA	CDMA	CDMA	CDMA
Switching	Circuit, packet	Packet	All packet	All packet
Core network	Packet Switch Telephone	Packet N/W	Internet	Internet

	Network (PSTN)			
Handoff	Horizontal	Horizontal	Horizontal and vertical	Horizontal and vertical

All of the above points to the need for effective understanding and measurement of EMF in each new generation, that will enable monitoring the intensity of EM radiation, all with the aim of maintaining the level of radiation within safety limits. Considerable research has been made in the area of potential hazards of EM radiation on humans [25, 26, 27]. Despite standards set, absorption of EM radiation in biological tissues has been, and continues to be, a public concern, especially for 5G networks. Having this in mind, the next chapter is devoted to the description of interaction between human being and EMF.

3 Interaction of High Frequency fields with living material

3.1 Interaction mechanisms

Electromagnetic fields are emitted by many human-made and natural sources daily, and the introduction of new frequencies and new technologies, especially in latest 5G, affects the human exposure to the radiation of these systems. Every day across the world, more than 3 billion people are exposed to EMF [28] and with new generation of mobile technology, it is necessary to design new methods for analysis of human exposure to EMF [24].

The interaction of EMF with materials depends on their frequency. One of the biggest obstacles for the implementation of 5G systems in the period from 2020 to 2025 are the issues related to radio frequency (RF) EMF [19]. Namely, the public is very concerned about the negative effects that may appear as a result of the wide implementation of the 5G system, especially in higher frequency bends. This concern relies on the fact that mm-waves are best absorbed by human skin, and wavelengths of RF EM waves are comparable to dimensions of the human organs, so thermal effects become dominant.

Depending on the characteristics of the source the potential consequences of EMF on human health are diverse. In the literature the effects of EM radiation on the human body or on its parts, are most often observed in different frequency bands, where most research of EMF are focus on effects observed in the area of eyes, skin tissue, and brain [29]. These potential effects will be explained later in this chapter.

In order to assess the environmental impact and health implications of EM waves, quantitative description of the EMF and power deposition in the tissues needs to be analyzed. EM waves can penetrate into the human body. The penetration or skin depth is considered as the depth at which the amplitude of EM field is attenuated by a value of 1/e (0.36) [30]. The intensity of EMF in the human body decreases exponentially from the surface to the interior of the tissue, which can be mathematically described by relation [30]:

$$I(z) = I_0 e^{-\alpha z} \qquad (3.1)$$

where

- I describes the EM wave intensity [V/m] as a function of depth z,
- I_0 is the intensity at the surface, and

- α is the attenuation coefficient in Np/m.

The penetration depth is a function the frequency of EM waves, the strength of the field and the electrical and dielectric properties of the human body [30]. The penetration depth is smaller at higher frequencies, that is, it is inversely proportional to the frequency of the incident wave. The higher the frequency of the EMF the stronger the absorption at the human body surface, therefore the higher the frequency the shorter the distance the field can penetrate into the human body. EM waves at frequencies around 3.5 GHz penetrate less into the muscle tissue in comparison with the waves of 2G and 3G systems [30], and despite bulky public concern adverse health impacts of EMFs radiated at 5G frequencies were not found [32-37].

The dielectric and electrical properties of the human body depend of the composition of the tissues in the human body. Water, fat, protein and salt content take part in the formation of dielectric properties of biological tissue. Dielectric constant and conductivity, play an important role in determining the energy deposition and hence, temperature elevation in biological matter [31]. Essentially, the amount of water in the tissue is the most important factor, so tissues are classified into tissues with a high percentage of water in their composition (eyes, muscles, skin, liver, and kidneys), tissues with a medium percentage of water in their composition (brain, shoulders and bone marrow) and those with a small percentage of water in their composition (fat and bones) [31]. Complex valued relative permittivity and conductivity of biological tissue are frequency dependent and the process are characterized as dispersion [31].

$$\varepsilon^*{}_r = \frac{\varepsilon^*}{\varepsilon_0} = \varepsilon_r' - j\varepsilon_r'' \qquad (3.2)$$

$$\sigma^* = j\omega\varepsilon^* \qquad (3.3)$$

where

- $\varepsilon^*{}_r$ Complex valued relative permittivity,
- $\varepsilon_r' = \frac{\varepsilon'}{\varepsilon_0}$ real part of complex valued relative permittivity,
- $\varepsilon_r'' = \frac{\varepsilon''}{\varepsilon_0}$ imaginary part of complex valued relative permittivity,
- ε_0 is the vacuum permittivity,
- σ^* is conductivity, and
- ω is the angular frequency.

Dispersion α occurs at low frequencies (LFs) due to ion diffusion on cell membranes [38]. Due to the polarization of cell membranes, proteins and other organic molecules, in the range of hundreds of kilohertz, β dispersion occurs [38]. In the gigahertz range, γ dispersion occurs as a result of the polarization of water molecules in the tissue [38]. Predicted decrease of Skin Relative Permittivity vs Frequency increase by different researches, and Conductivity increase vs Frequency increase is shown in Figure 3.1. (a) and Figure 3.1. (b) [30]. Figure 3.2. shows changes in the penetration depth of some organs in relation to the frequency of the incident wave [31].

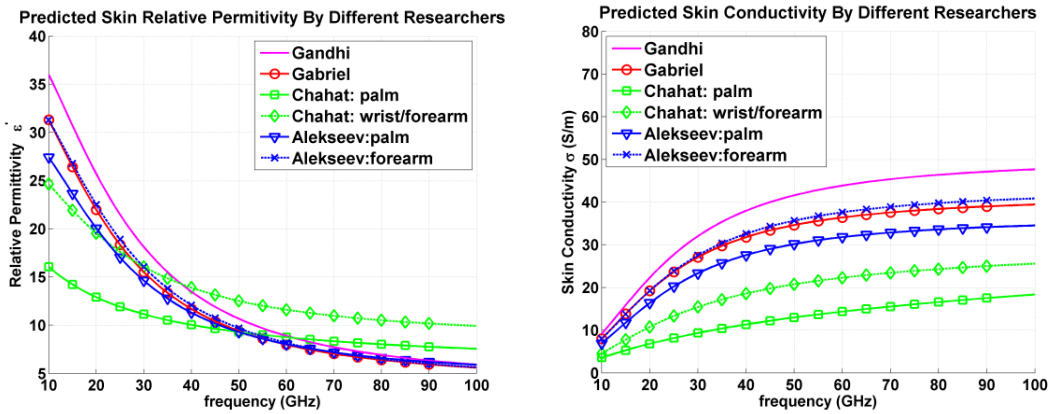

Figure 3.1. (a) Relative permittivity vs frequency (b) Skin Conductivity vs frequency [30]

Adipose tissue and bones have low conductivity, because they have a small percentage of water [30].

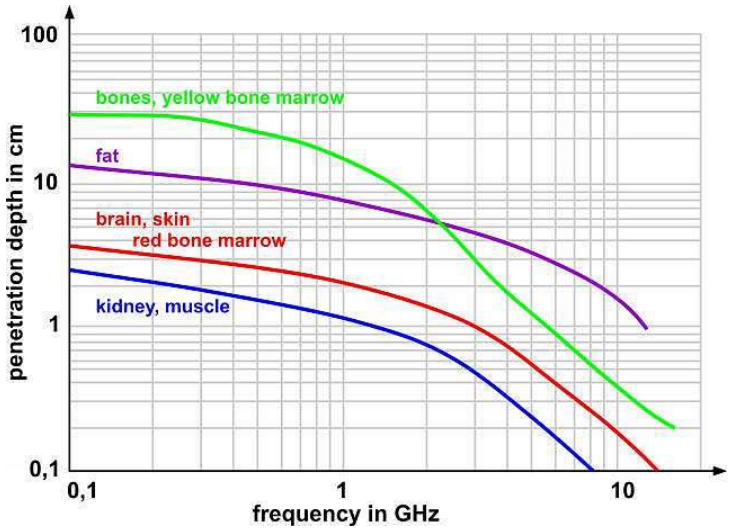

Figure 3.2. Variation of the penetration depth of few organs as a function of frequency [31]

Bone conductivity is very low, about 0.3 S/m at 1.8 GHz, compared to approximate Value of thermal conductivity 0.488 W/mK [39], so the penetration depth is about 8 cm (Figure 3.2.) and drops by more than 72 % at 3.5 GHz [31] (2.2 cm). Brain and lean tissues have a smaller

penetration depth, which decreases from 1.7 cm at 1.8 GHz to 0.85 cm at 3.5 GHz [31]. Muscles are the best at absorbing EM waves and very efficiently dissipate energy into heat.

3.2 Biological effects

Due to the use of a large number of electronic devices in everyday life, the human body is exposed to radiation of EM waves of different frequencies (Figure 3.3.). As the frequency of the EM energy spectrum changes from extremely low to Gamma rays, the effects of EMFs on humans also change [40].

Extreme LF (ELF) and Very LF (VLF) frequency band induce non-thermal effects, while LF, Medium Frequency (MF), HF, VHF, Ultra HF (UHF) bends lead to heat generation (thermal effects). EMFs on aforementioned frequencies cause non-ionizing radiation. Thermal effects are associated with the heat created by EMFs in a certain area, and it is possible that every interaction between RF fields and living tissues causes an energy transfer resulting in a rise in temperature [28].

On the other hand, at ultra violet, X-Ray and Gamma Rays frequency band ionizing radiation may lead to different non-thermal effects, such as Deoxyribonucleic acid (DNA) damage, cancer, mutation and birth defects.

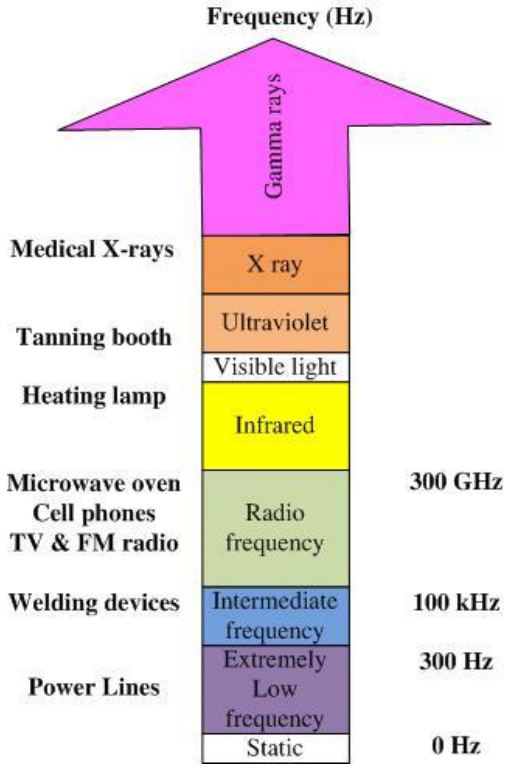

Figure 3.3. EM spectrum

Generally excessive exposure to EM radiation leads to various physical sensations grouped into Short-Term Health Effects, Long-Term Health Effects and Electrical Sensitivity, as shown in Table 3.1.

Table 3.1. The non-thermal effects of EM fields on human body

Short-Term Health Effects	**Long-Term Health Effects**	**Electrical Sensitivity**
Aches and pains	Cancers	Sleeping problems
Headaches	Brain Tumors	Cognitive impairment
Decrease sperm motility	Fragmented DNA	Concentration or memory loss
Tingling or burning sensations	Mutated cells	Brain Fog
Anxiety, stress, Neurological irritability		

The population living near sources of radiation of EMFs is more prone to the development of various health risks, such as depression, headaches, memory loss, irritation, sleep disorders, loss of appetite, dizziness, vision loss and cardiovascular disorder [41-42]. Excessive exposure to EM radiation has a significant impact on sperm quality [43-46]. It also affects the fertility rate of women by changing the shape of the ovaries and the loss of eggs.

Since the entire human body is covered with skin, EMFs interact with the human body through the skin, and during interaction one part of the HF EMF wave is reflected, and the other part is absorbed by the skin. About 40% of the incident power is reflected on the surface of the skin, and the remaining 90% of the power is absorbed in the epidermis and dermis layer of the skin. Depending on gender, skin, human body type, hydration level and skin thickness, a different amount of EM waves will be absorbed. Bare skin absorbs radiation better [47]. However, due to the low incident power, the wave penetration is not deep, so the human skin can only create a thermal effect on the human body [36]. A modest localized heat exposure can be compensated by the human body's heat regulation system. High doses of absorbed RF exposure leads to generation of oxidative stress, DNA adducts and cancer. [48].

Due to the high bandwidth of the 5G network, chromosome aberrations or cell mutations can occur, thus forming tumors that can later become malignant (Figure 3.4.) [49].

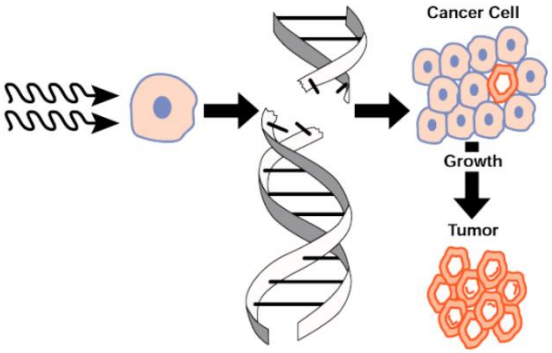

Figure 3.4. Cancer form due to radiation [50]

High levels of RF exposure with sufficiently high-power density may cause several ocular effects [50], including cataracts (Figure 3.5.), retina damages, and cornea issues.

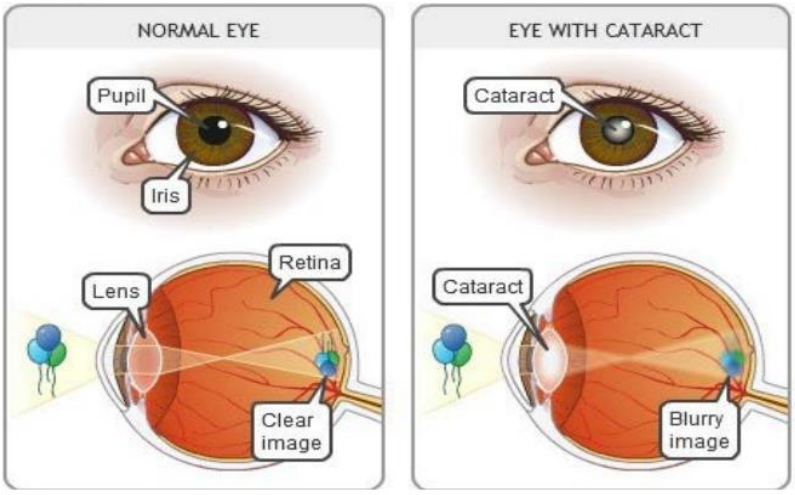

Figure 3.5. Formation of cataracts [50]

As a result of excessive exposure to EM radiation from the 5G spectrum, EM sensitivity, with symptoms such as: headache, insomnia, dizziness, fatigue, loss of focus, palpitations and exhaustion, can occur [48, 51-53].

3.3 Safety Guidelines

Various organizations have proposed guidelines for limiting exposure to EMFs for protection against all established adverse health effects. The most used limits are defined by ICNIRP [54, 55] and by IEEE [56]. Guidance are given in terms of basic restrictions (BRs) and/or reference levels (RLs) (Fig. 3.6.). BRs are exposure indices within the body that should not be exceeded, and are specified in terms of non-measurable internal electric field [55] and the current density in LF range. The rate of RF energy absorption (Specific Absorption Rate, SAR) [55] is the BR specified for HF range.

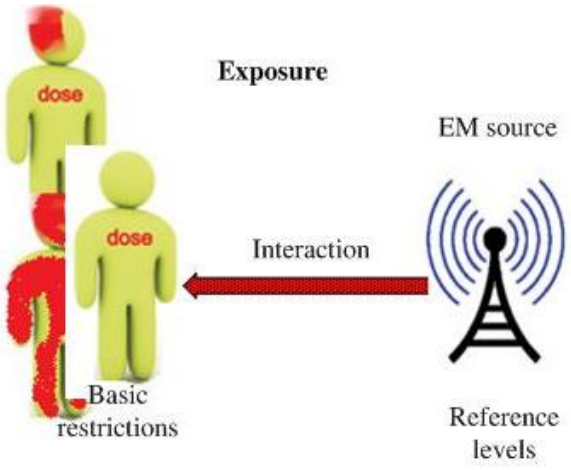

Figure 3.6. Quantities in the guidelines: basic restrictions on the internal dose and reference levels for the external exposure.

Since measurements of the SAR or internal electric field strength are often difficult to perform, RLs for maximum human exposure to RF fields have also been specified. The RLs are specified in terms of unperturbed, externally applied electric and magnetic field strength, power density and in terms of electric currents in the body occurring from either induction or contact with energized metallic objects. While compliance with the BRs is required, non-compliance with the RLs does not necessarily mean that the BRs are not respected. In such cases, additional measurements or calculations may be required to assess compliance. Further on, we will mainly discuss BRs, but additional information about RLs are offered in [54,55].

BRs are frequency dependent dosimetric quantities. For 3 kHz–10 MHz frequency range BRs for the avoidance of non-thermal effects are specified in terms of maximum internal electric field strength within the body [54,55]. In the frequency range from 100 kHz to 300 GHz tissue heating must be restricted. Bellow 6 GHz limits are defines using specific energy absorption rate in terms of maximum whole-body SAR (averaged over the whole-body) and peak spatially-averaged SAR (averaged over a small cubical volume) [55]. Above 6 GHz, EMFs are absorbed more superficially, and exposure is described in terms of reference levels for maximum unperturbed, externally applied electric and magnetic-field strengths and in terms of power density.

The threshold value of whole-body average SAR that causes a core body temperature change of ~1.0 ℃ is ~ 4 W/kg, according to the results of numerous previous studies conducted on animals [57-59]. Adverse health effects may appear when temperature elevation is between 1-2 ℃ [60]. With the incorporation of the safety factor, a whole-human body average SAR of 0.4 W/kg has been chosen as the restriction that provides adequate protection for occupational

exposure [55]. An additional safety factor of 5 is introduced for exposure of the public, giving an average whole-human body SAR limit of 0.08 W/kg [55].

The BRs defined in [55] are particularly important for our future research, since they cover the HF frequency range. Specifically, sub 6 GHz frequency spectrum, which is also one of the most used for latest generation of mobile technologies, and in which the main dosimetric quantity is SAR. Research done in [61] shown that the maximum value of the electric field magnitude, the SAR, and the temperature increase can be seen at 3 GHz, which makes this frequency very attractive for analyze.

Due to the different thermoregulatory properties of different tissues in the human body, peak spatially-averaged SAR limits (1 or 10 g, in the shape of a cube) for exposures in controlled environments are 20 W/kg for the limbs and 8 W/kg for the head, neck and trunk. For exposures in uncontrolled environments, the peak spatially-averaged SAR limits are 4.0 W/kg for the limbs and 1.6 W/kg for the head, neck and trunk [56].

3.4 Dosimetry – General Aspects

To reach its intents, dosimetry relies on theoretical or experimental techniques, and the process is done true three steps: incident field dosimetry, internal field dosimetry and thermal field dosimetry. Electromagnetic dosimetry represents the quantification of energy absorbed by an object (such as human body or it's part) exposed to HF EMFs, where the fundamental step is the evaluation of external EM field distribution [57]. In EM dosimetry, the absorbed energy is determined by the internal EM fields that are induced by external (incident) EM energy. The external and internal fields are very different and are interrelated by the EM field boundary conditions (BCs) and wave transmission theory [58]. Electromagnetic dosimetry encompasses incident field dosimetry and internal field dosimetry.

External field distribution evaluation starts by observation and modelling of environmental sources. In this sense, environmental sources are the source antenna and transmission system. Given that simplified methods are based on the introduction of approximations, the authors proposed different theoretical methods of incident field dosimetry such as: Norton model short VED at the surface of the earth, Wait model for line current source above the ground, King model for VED at height d in air, Kurniawan and Wood model, analytical model for broadband Power line communication (PLC) by Chaaban, Drissi, and Poljak and Parise model. A more

detailed description is given in chapter 4.1.. According to the differential and integral formulation of the problem, domain, boundary or source simulation numerical methods can be used.

The induced field is the primary source of energy driving the interaction of the EM energy within the biological system. Although it may contribute to the formulation of mechanisms of interaction, it is independent of any mechanism of interaction. The coupling mechanisms of the electric and magnetic incident-field components are different. Hence, both must be determined separately to fully characterize human exposure. Since coupling with the human body also depends on the ratio of wavelength versus body size, the RF-EMF spectrum is often divided into at least three ranges, e.g. 30 kHz–10 MHz (below body resonance); 10 MHz to 2 GHz (body and partial body resonances); and 2 GHz to 300 GHz (surface-dominated absorption) [48]. Furthermore, the distribution of the induced field strongly depends on various parameters, such as source (strength, frequency, polarization, direction of incidence, size, shape, etc.), distance and location of the source with respect to the body, outer anatomy, inner anatomy, body posture, and environment of the body (e.g. reflective objects). For the application of simplified models, internal field dosimetry simplified human body models must be used. The most commonly used simple models of the human body are the spherical, parallelepiped and cylindrical models. Phantoms simulating the human body or parts play a central role in EM dosimetry. Phantoms are physical or computational.

The field variations within the body are generally appreciable and may well exceed a factor of thousand for the locally absorbed energy. In general, field distributions change considerably between different postures and orientations of the body with respect to the field. For example, the exposure of the brain may change even though the whole-body average and the peak spatial absorption remain the same. Induced currents and fields may give rise to thermal and non-thermal effects, and in HF range thermal effects are dominant. The basic dosimetric quantity is SAR, and as direct experimental measurements of thermal response on healthy human subjects is not possible, many computational studies aim to relate SAR and temperature elevation in human body.

Third step in dosimetry is thermal field dosimetry where numerous models can be used to describe the process of heat exchange, but the model proposed by Penne's is widely used. The analytical solution using the Laplace Transform method, A Method based on modified Penne’s

Bioheat Equitation (PBE), method based on Bessel functions, the method based on Green's function are often used and the method based on Separation of Variables (SoV) are often used in analyzed literature. Even analytical methods are preferable in this step, some of the numerical approaches used to solve PBE are Boundary Element Method (BEM), the Finite Element Method (FEM), the Finite Difference Method (FDM), the Dual Reciprocity BEM (DRMBEM), the Monte Carlo method (MCM), and the Meshless method.

Research on the impact of EM radiation on the human body is based on the measurement of standardized dosimetric quantities and their comparison with defined limits. The dose of absorbed EMF energy is dependent of frequency. If the measured/calculated quantity is above the permissible limit, short-term/long-term effects of this exposure may occur. Even in the case of the mentioned effects, the studies are divided. Some have proven the existence of these effects, but the influence is mostly experimentally unconfirmed.

4 Incident Dosimetry Methods

Incident EMFs are defined as external fields in the absence of – i.e. without interaction with – the human body, animals, or tissue samples. Incident fields couple with the human body and induce EMFs and currents inside the body tissues. The induced fields are the only exposure parameters that can interact with biological processes and, therefore, provide the primary exposure metric [59].

One of the simplest scenarios to assess the human exposure to HF radiation is the human body exposed to the EMF radiated by thin wire antenna. Even with the new technologies coming along a simple human body model exposed to dipole antenna radiation [60, 61] is of interest for quick dosimetry procedures, aiming to get a rapid estimation of the phenomena.

EM modelling of the radiation from vertical electric dipole (VED) antenna above a lossy half space usually points the problem towards solving Sommerfeld-type integrals that represent the effect of the media interface. The traditional solution of the classical Sommerfeld problem uses Hertz potentials which cannot be evaluated in a closed form. Generally, because Sommerfeld-type integrals are infinite, they are highly oscillatory [62], difficult to evaluate numerically [62] require intensive computational resources, and the accurate evaluation of Sommerfeld integral expressions is not a straightforward task [63]. This complexity leads to development of numerous approximations, but the only feasible approach for obtaining a reliable, straightforward solution has been to integrate the Sommerfeld integrals numerically [64].

The first step in calculating the electric and magnetic fields generated by wire antennas is to determine the current distribution along the wire. The current distribution along the wire is governed by electric field integral equation (EFIE) for thin wires, known as the Pocklington's integro-differential equation. Furthermore, numerical solution of Pocklington equation is demanding per se in a sense of accuracy, convergence and kernel quasi-singularity [65, 66]. Therefore, some analytical simplifications, such as [67], under certain conditions are always welcome. Besides aforementioned analytical and numerical techniques, the problem of quantification of the interaction of EM waves within the exposed human body can also relay on experimental approaches, as shown in Figure 4.1. [67].

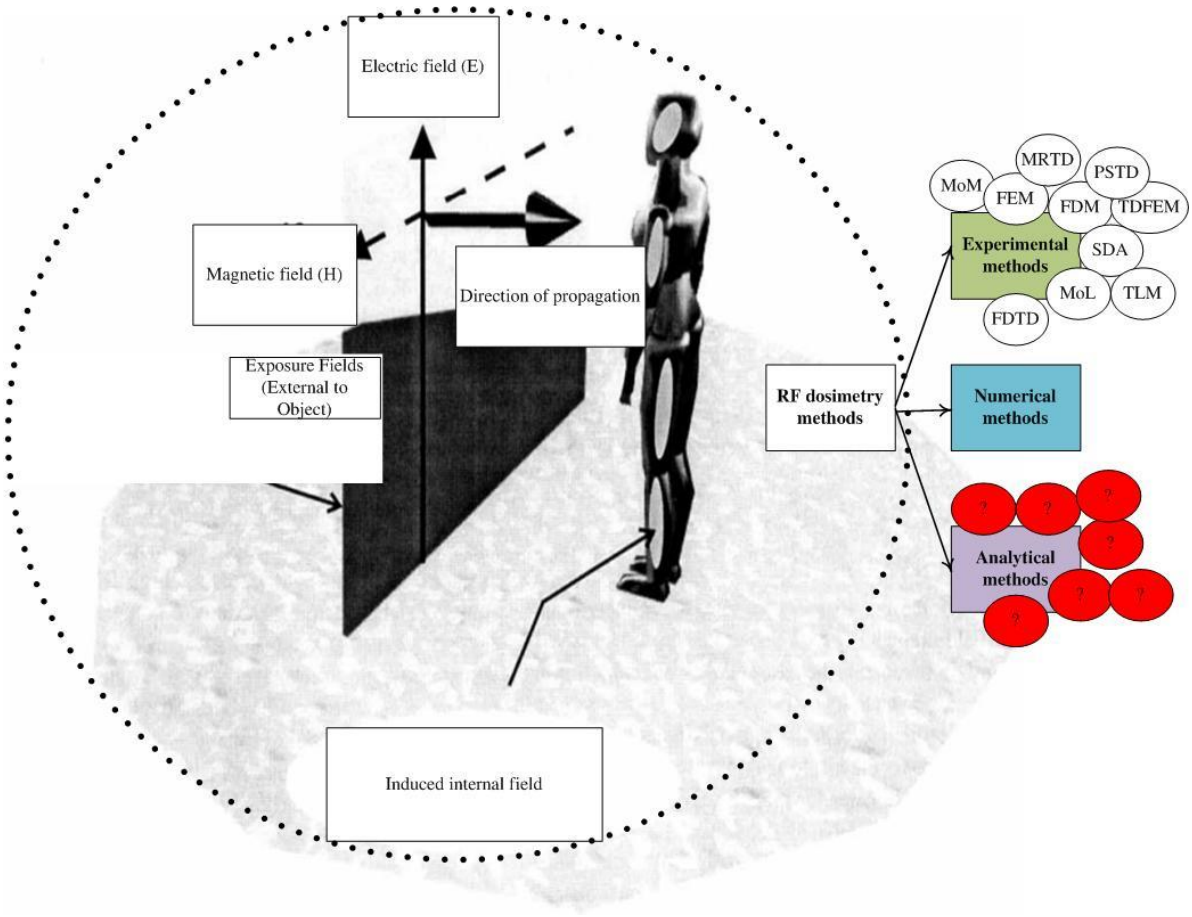

Figure 4.1. Different methods for electromagnetic-thermal dosimetry [37]

As analytical methods offer simplicity, and reduce computational cost they are valuable tool in many applications of EM dosimetry. The focus of this chapter is to give a short review of analytical techniques.

4.1 Literature review

1930s: ***Norton model short VED at the surface of the earth (Figure 4.2.)***. On Sommerfeld EMF radiated by an infinitesimal VED located on the surface of the planar Earth, Norton introduced the attenuation function, the ground effect, and the frequency dependence of the surface wave. Norton's formalism starts from the Hertz vector composed of a direct wave, a reflected wave (the sum is also called space wave) and the surface wave [68].

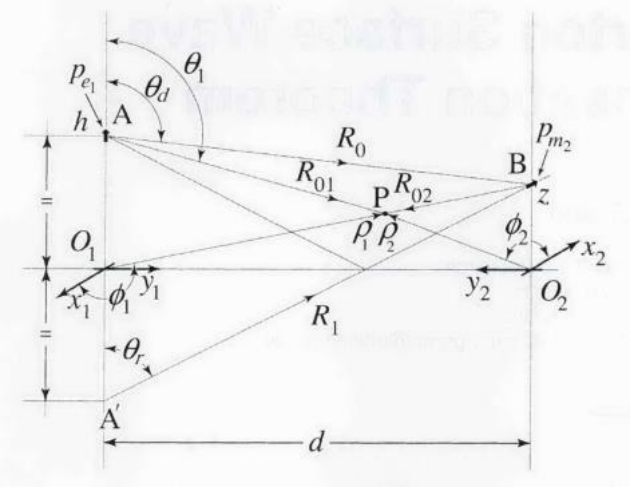

Figure 4.2. Norton model [69]

For small angles and short distances, the surface wave term must be used together with direct wave and reflected wave. As the distance is increased, the direct wave and reflected wave are sufficient for the specification of the field. Norton in his effort to simplify the expressions developed by Sommerfeld, derived equations that clearly show the surface wave and space wave components and works only in the far-field regions [68, 70].

1960s: Wait model for line current source above the ground (Figure 4.3). The EM fields created by phased line current over a conducting half space are analyzed by Wait.

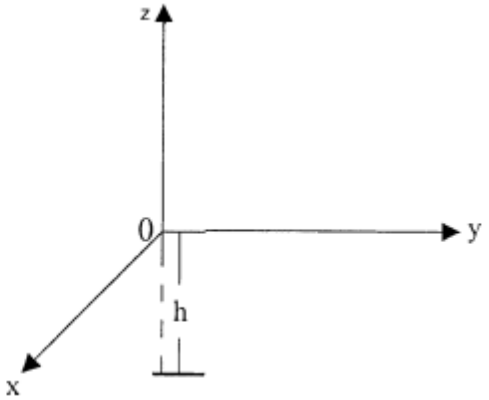

Figure 4.3. Equivalent excitation coil circuit [71]

In the quasi near-field region, the field in the air due to the flow of currents induced in the ground can be described using a modified image theory (MIT). Namely, in this region, the distance from the radiating object is small compared to the wavelength, but large enough compared to the skin depth in the ground [72]. According to MIT, reflection coefficient is given as [72, 73]:

$$R_{MIT} = \frac{\varepsilon_{eff} - \varepsilon_0}{\varepsilon_{eff} + \varepsilon_0} \qquad (4.1)$$

$$\varepsilon_{eff} = \varepsilon_r \varepsilon_0 - j\frac{\sigma}{\omega}\left(\frac{F}{m}\right) \qquad (4.2)$$

where

- $\varepsilon_{eff}[\frac{F}{m}]$ describes the effective permittivity.

Therefore, the reflected and total electric field, respectively:

$$E_{MIT}^{R} = R_{MIT} * E_{MIT}^{Inc}\left(\frac{V}{m}\right) \qquad (4.3)$$

$$E_{MIT}^{Tot} = E_{MIT}^{Inc} + E_{MIT}^{R}\left(\frac{V}{m}\right) \qquad (4.4)$$

where

- $E_{MIT}^{R}[V/m]$ describes the reflected electric field component
- $E_{MIT}^{Inc}[V/m]$ is a direct electric field component, and
- $E_{MIT}^{Tot}[V/m]$ is the total electric field.

Wait model is purely analytical technique and it is important contribution since presents field expressions derived through usage of the complex image theory. The only drawback of the obtained formulas resides in that they are valid in the quasi-static regime only, that is when the effects of the displacement currents in the air space are negligible [70].

1980s: King model for VED at height d in air (Figure 4.3.). In order to remove the restrictions for the application of the Norton and Wait models for the field of dipole over imperfectly conducting ground, in 1982 King formulated a set of equations valid everywhere in the earth and on boundary when the dipole is also on the boundary in either in either region or at depth d in the earth:

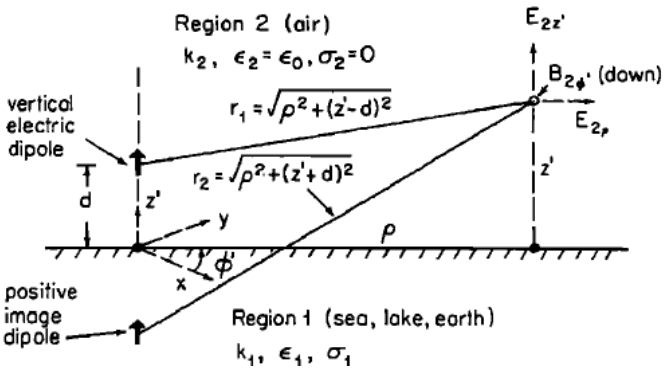

Figure 4.3. Vertical electric dipole at height d in region 2 [74]

The conditions for applying the model are [75-81].

$$|k_1^2| \gg k_2^2 \text{ or } |k_1| \geq 3k_2 \qquad (4.5)$$

where

- $k_1 = \omega\sqrt{\left[\mu_0\left(\varepsilon_1 - j\frac{\sigma_1}{\omega}\right)\right]}$ is the wave number of lower half space (earth, z<0),
- μ_0 is vacuum permeability, and
- $k_2 = \omega\sqrt{\mu_0\varepsilon_0} = \frac{\omega}{c}$ is the wave numbers of upper half space (air, z>0).

When the radial distance (ρ) is large compared the height (d) of dipole or height z of the observation point (4.6), King model uses phase approximations (4.7, 4.8 and 4.9) and amplitude approximations (4.10):

$$\rho^2 \gg (z-d)^2 \; \rho^2 \gg (z+d)^2 \qquad (4.6)$$

$$r_1 \sim r_0 - d\cos(\theta) \qquad (4.7)$$

$$r_2 \sim r_0 + d\cos(\theta) \qquad (4.8)$$

$$r_0 = \sqrt{\rho^2 + z^2} \qquad (4.9)$$

$$r_1 \sim r_2 \sim r_0 \qquad (4.10)$$

Using these simplifications, the total electric field on the earth's surface is determined primarily by the lateral surface wave, since the space wave vanishes there [75].

2000s: **Kurniawan and Wood model (Figure 4.4.)**. The method takes into account the heuristic simplification in calculation of near EMF.

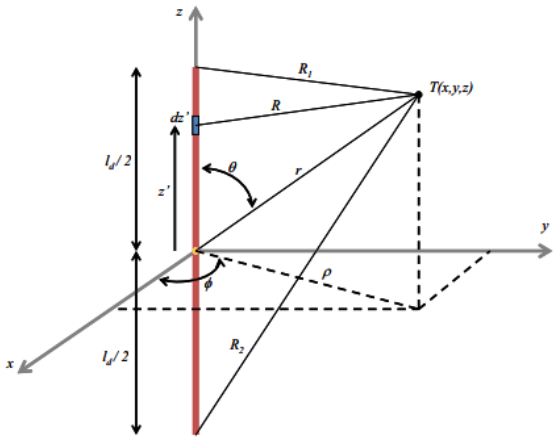

Figure 4.4. Equivalent excitation coil circuit [82]

Simple closed-form analytical formulas of near fields from free space thin finite length dipole are multiplying with correction factors (c_s or c_{fl}), and the calculations are valid in lossy homogeneous medium [82]. Correction factors to compute the induced near electric field E are introduced heuristically:

$$c_s = \left|\frac{k_L}{k_h}\right| = \left[\frac{1}{\sin\left(\frac{|k_L| l_d}{2}\right)}\right] \tag{4.11}$$

$$c_{fl} = \begin{cases} \left|\frac{k_L}{k_h}\right| & for\ 0.75 < \left|\frac{k_L}{k_h}\right| < 0.95 \\ e^{-0.002\left|\frac{k_h}{k_L}\right|\frac{\lambda}{\rho}} & for\ \left|\frac{k_L}{k_h}\right| < 0.75 \end{cases} \tag{4.12}$$

where

- k_L the is wavenumber for the insulator (that accounts for the lossy dielectric medium surrounding antenna),
- k_h ($k_L < k_h$) is the wavenumber of ambient lossy dielectric medium,
- l_d is the dipole length,
- λ is wavelength, and
- ρ is radial distance.

For $\frac{k_L}{k_h} > 0.95$ correction factor is 1 (because results differ insignificantly) [82].

Analytical model for broadband Power line communication (PLC) by Chaaban, Drissi, and Poljak (Figure 4.5.).

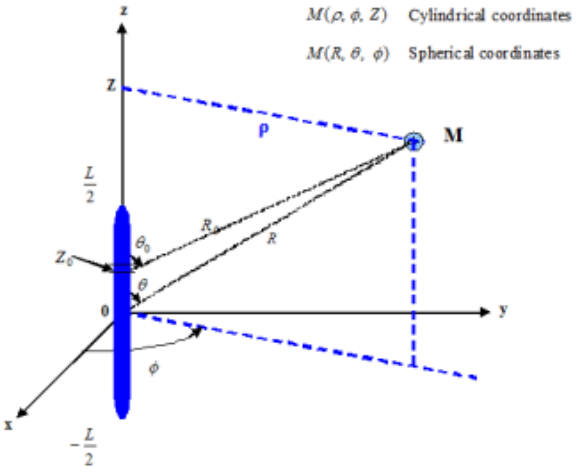

Figure 4.5. Radiating antenna in free space [83]

Authors proposed an analytical approach to evaluate EMF radiated from thin-wire structures. The advantages of this approach are rapid estimation of the phenomena and simplicity. Prerequisite is knowing the values of the currents and voltages (derivates of the current) at the line ends [83]. The mathematical model for EMF calculation is based on integral equitation formulation in frequency domain. Knowing current distribution along the wire is the first step to EMF calculation [80]. In this approach authors assumed spatial current distribution, and electric and magnetic fields in spherical and cylindrical coordinates are given.

A line of length L and radius a (a<<L) is directed at the z-axis direction (YZ plane), where the observation point is at a distance R measured from the center of the cable [83].

$$\gamma = \frac{j\omega}{v_1} = j\beta_1 \qquad (4.13)$$

$$\gamma_0 = \frac{j\omega}{c} = j\beta_0 \qquad (4.14)$$

where

- γ_0 is the propagation constant in free space,
- γ ($\gamma a << 1$) is the propagation constant of the PLC,
- c is the speed of light, and
- v_1 is the speed in line.

The line is segmented into an infinite number of elementary dipoles (with positions at the point $M_0\,(0,0,Z_0)$ through which the current $IM_0(s,\ Z_0)$ flows. Radial and tangential electric field components accompanied by an azimuthally component of the magnetic field expressed in terms of axially dependent magnetic vector potential:

$$\mathrm{E_z} = -\frac{\mathrm{j\omega}}{\beta_0^2}\left(\frac{\partial^2 \mathrm{A_z}}{\partial \mathrm{z}^2} + \beta_0^2 \mathrm{A_z}\right) \qquad (4.15)$$

$$\mathrm{E_\rho} = -\frac{\mathrm{j\omega}}{\beta_0^2}\frac{\partial^2 \mathrm{A_z}}{\partial \rho\, \partial \mathrm{z}} \qquad (4.16)$$

$$\mathrm{H_\varphi} = -\frac{1}{\mu_0}\frac{\partial \mathrm{A_z}}{\partial \rho} \qquad (4.17)$$

$$\overrightarrow{\mathrm{A_z(p)}} = \frac{\mu_0}{4\pi}\int_0^{\mathrm{L}} \mathrm{I(p,z)}\frac{\mathrm{e}^{-\gamma_0 \mathrm{R(z)}}}{\mathrm{R(z)}}\,\mathrm{dz}\vec{\mathrm{z}} \qquad (4.18)$$

where

- $I(s, z_0)$ is the current distribution along the conductor, and

- $R(z) = \sqrt{\rho^2 + (z - z_0)^2}$ is the distance between the elementary dipole and the observation point M,

This model is valid in near and far field and radiated fields are expressed only in terms of current and its derivatives (voltages) at the line ends. By using this model, the computational cost may be reduced.

Nazari and Huang model (Figure 4.6.). Nazari and Huang introduced a new method by breaking down the intermediate Hertz potential into three terms. The two term of the Hertz potential associated with the Sommerfeld integrals are expressed using hyperbolic functions, and the third term is approximated using Saddle Point Method (SPM) [84].

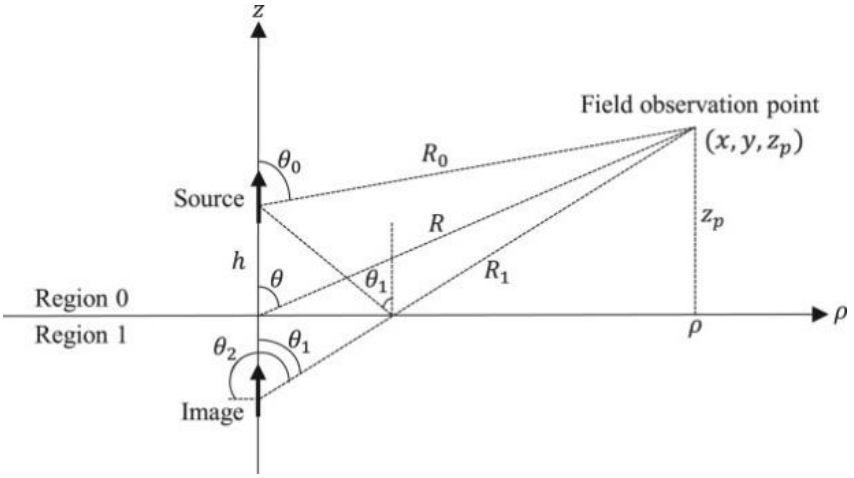

Figure 4.6. Dipole source above a lossy half space. [84]

SPM of integration approximates Sommerfeld integrals in far field regions, in which the distance between the antenna and the observation point is considerable. However, for a lossy half-space problem, the SPM method is not capable of approximating Sommerfeld integrals since the Sommerfeld pole is close to the saddle point for this problem. The solution for electric field equitation, defined by Nazari and Huang is asymptotic and outperforms the conventional solutions, such as King and Norton solutions, in terms of Normalized Root-Mean-Square Error (NRMSE) and Normalized Maximum Absolute Error (NMAE) at various frequencies and distances from the antenna in the far field region [84]. Authors compared their new method to King and Norton solutions, and the rigorous numerical computation done with the high-order global adaptive quadrature method.

NRMSE and NMAE of the proposed solution are lower than the conventional solutions for both scattered E and H fields [81]. Further on, the proposed solution agrees well with the numerical solution, particularly in high angles and near the interface, and proposed solution is more

accurate than the King and Norton solutions. However, this solution is only applicable for LF, highly conductive surfaces and far field regions. It is worth mentioning that the accuracy and efficiency of all aforementioned methods are limited by the antenna and observation point locations and EM properties of each medium, that is, permittivity and conductivity of the regions.

Parise model (Figure 4.7.). The components of the time-varying EM field radiated by the line source with uniform current distribution located above a homogeneously dissipative ground (Figure) can be expressed in a rigorous series form.

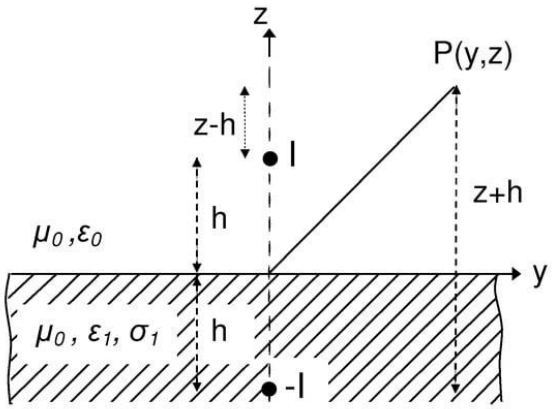

Figure 4.2. Sketch of a line source of current above a homogeneous ground. [85]

Total electric field generated in the air space has only one component in the axial direction and can be derived by decomposing the integral expression for the axial component of the electric field into the direct field induced by the source current, the ideal reflected field induced by the negative image and a correction term due to the imperfect conductivity of the ground [85]. The advantage of this solution is that it does not introduce any simplifications, so it is valid in case displacement currents in both the air and the soil are not negligible. Further on, this solution requires less computation time than conventional numerical quadrature schemes used to evaluate Sommerfeld integrals. For this method, the line source needs to have uniform current distribution.

A summary of ongoing research in this field with a basis of the author's research with benefits and limitations of their solutions is shown in Table 4.1. It can be noticed that one of the simplest scenarios which can be used to assess human exposure to HF radiation is one where the human body is exposed to the EMF radiated by a thin wire antenna. A simple dipole antenna combined with a simple human body model is often used for quick dosimetry procedures, aiming to get a rapid estimation of the phenomena.

Table 4.1 Summary of ongoing work in these field

Year	Authors	Base of the work	Benefits	Limitations
1936	Norton	Usage of long algebraic expressions for engineering use, in which the so – called 'attenuation coefficient' for the propagating surface wave plays an important role	Formulas valid for any frequency and set of ground constraints	Formulas limited to UHF frequency band
1969	Wait & Spies	Field expressions derived through usage of the complex image theory	Pure analytical solution (less memory requirements and computational costs)	Valid in the quasi-static regime only (when the effects of the displacement currents in the air space are negligible)
1982, 1990, 1994, 1995	King, et al.,	Formulas are made of exact expressions for direct and reflected filed, and approximate formula expression for Norton surface wave	Remove the restrictions for the application of the Norton and Wait models	Valid in far field zone
2010	Kurniwan & Wood	Simple closed-form analytical formula of near fields from free space thin finite length dipole are multiplying with correction factors, so the calculations are valid in lossy homogeneous medium.	Simple closed-form analytical solution with satisfying accuracy	Valid for following assumptions: free space surroundings, sinusoidal current distributions, centre-fed dipole with infinitesimal gap, PEC material for the dipole, and fed by RF band signals
1982, 1990, 1994, 1995	King, et al.,	Formulas are made of exact expressions for direct and reflected filed, and approximate formula expression for Norton surface wave	Remove the restrictions for the application of the Norton and Wait models	Valid in far field zone
2010	Kurniwan & Wood	Simple closed-form analytical formula of near fields from free space thin finite length dipole are multiplying with correction factors, so the calculations are valid in lossy homogeneous medium.	Simple closed-form analytical solution with satisfying accuracy	Valid for following assumptions: free space surroundings, sinusoidal current distributions, centre-fed dipole with infinitesimal gap, PEC material for the

				dipole, and fed by RF band signals
2012	Chaaban, Drissi, & Poljak	Authors assumed spatial current distribution, and electric and magnetic fields in spherical and cylindrical coordinates are given.	Rapid estimation of the phenomena and simplicity; Valid in near and far field Radiated fields are expressed only in terms of current and its derivatives (voltages) at the line ends.	Knowing the values of the currents and voltages (derivates of the current) at the line ends.
2020	Nazari & Huang	An approximate closed-form solution of the far-zone scattered EMFs is calculated from the intermediate Hertz potential expressed in terms of the Fourier-Bessel transforms associated with the Sommerfeld-type integra using the modified saddle point method.	Normalized root-mean-square error and normalized maximum absolute error lower than the conventional solutions	Valid in far field region
2020	Parise	Decomposition of the integral expression for the axial component of the electric field into the direct field induced by the source current, the ideal reflected field induced by the negative image and a correction term due to the imperfect conductivity of the ground	Valid in case displacement currents in both the air and the soil are not negligible less computation time than conventional numerical quadrature schemes used to evaluate Sommerfeld-type integrals.	Line source has uniform current distribution.

By observing column 4 and 5 in Table 4.1. it can be concluded that analytical methods yield exact solutions, but are limited to a narrow range of applications, mostly related to canonical problems. By observing column 3 in Table 4.1. one can see that there are few practical engineering problems that can be solved in closed form [69]. An analytical method is used when a problem requires an accurate solution. Although analytical methods lead to accurate solutions

of formulas describing EMF, they can only be applied to very simple cases, namely thin antennas or simple radiating structures [72, 73], and therefore, their use is somehow limited.

The purpose of electromagnetic-thermal analysis is the calculation of dosimetric quantities and the comparison of calculated values with limits defined by Standards, with the aim of preventing harmful effects of EM radiation. The principal biological effect of HF fields has been considered to be dominantly thermal in nature. Namely, the hazardous EMF levels can be quantified analyzing the thermal response of the human body exposed to the HF radiation. Thermally harmful effects can occur if the total power absorbed by the human body is large enough to cause protective mechanisms for heat control to break down. This may lead to an uncontrolled rise in human body temperature (hyperthermia).

In order to be able to determine the impact of an EM field on a human organism, it is necessary to satisfactorily model the human body, that is, the human tissue. The term RF dosimetry, is related only to energy absorption in tissue, but not to the exposure of the human body to the external fields. The transfer of EM energy from an external source to tissue represents a complex function with many variables. EM interactions can produce highly nonuniform distributions of EM fields within the object, regardless of the external field uniformity exposure [37].

A variety of units can be used to express external incident field intensity. Exposure data can be expressed in terms of power density (W/m^3), or external electric field strength (V/m) and magnetic field strength (A/m). However, this data does not provide investigators with sufficient insight into how fields interact with biological tissue. On the other hand, a resulting thermal response of the human body due to exposure to HF radiation can be determined by possessing information about the internal electric field and related total absorbed power in the human body.

4.2 Incident Electric Field Dosimetry

The most common simplifications on the side of the radiation source refers to the representation of the antenna in the form of a Perfectly Conducting (PEC) wire, and the observation of the wave as flat, i.e. placing the model of the human body in the far field zone. The geometry of the problem is shown in Figure 4.2.

A vertical electric dipole (VED) antenna of length L, placed in the air along the z-axis, above a lossy half space at height h, is considered. The upper half space is free space. The resulting field

is the superposition of a direct field and earth-reflected field. VED antenna is assumed to satisfy the thin wire approximation [65]. The antenna is also assumed to be perfectly conductive, with current flowing along the surface in z direction and the current is supposed to vanish at the wire ends. The antenna parameters depend on the current distribution along the wire, which is obtained as a solution of the Pocklinton integro-differential equation in the frequency domain.

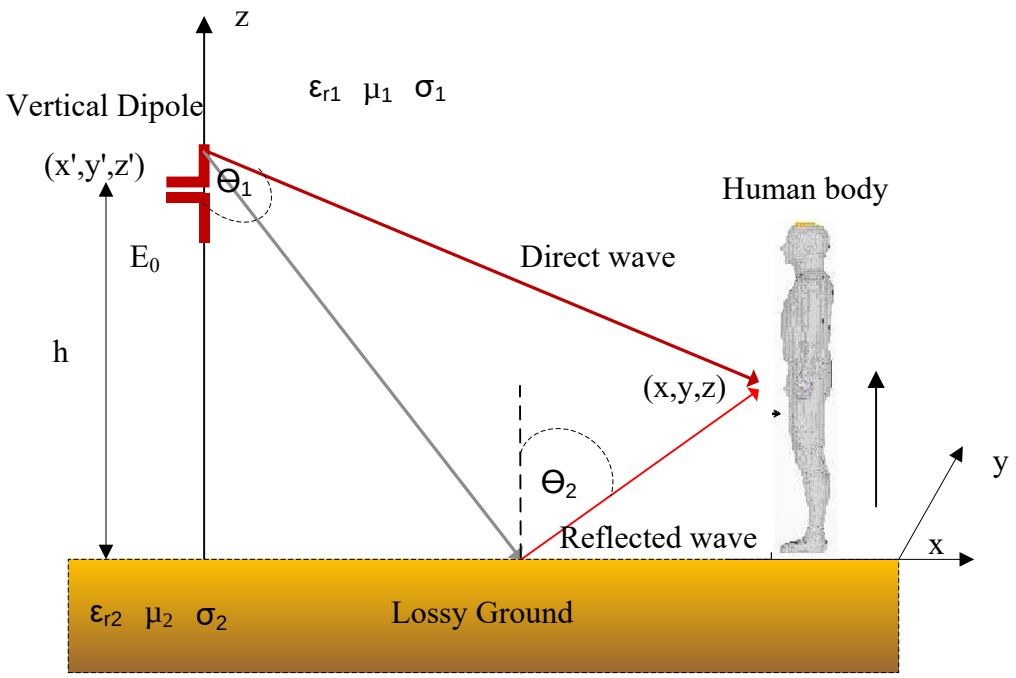

Figure 4.2. VED antenna above a lossy half space at height h [86]

This equation is obtained from Maxwell's equations by expressing a time-harmonic electric field by means of a vector magnetic potential and electric scalar potential

$$\vec{E}^{sct} = -\nabla\varphi - j\omega\vec{A} \quad (4.19)$$

where

- $\vec{E}^{sct}$ is scattered electric field,
- φ the electric scalar potential, and
- $\vec{A}$ magnetic vector potential.

By combining (4.19) with the continuity equation for potentials (4.20) and adopting the thin wire approximation, the electric field in the z-axis direction (tangential to the wire) is obtained (4.21).

$$\nabla\vec{A} = -j\omega\mu\varepsilon\varphi \quad (4.20)$$

$$E_z = \frac{1}{j\omega\mu\varepsilon_0}\left[\frac{\partial^2 A_z}{\partial z^2} + k_0^2 A_z\right] \quad (4.21)$$

where

- ω is the angular frequency,
- $\mu = 4\pi \times \frac{10^{-7}\mathrm{H}}{\mathrm{m}}$ is magnetic permeability,
- ε_0=8.854×10^{-12} F/m is the absolute permittivity in vacuum or air and
- k_0 is air wave number.

The particular solution of the vector wave equation of the vector magnetic potential is

$$A_z = \frac{\mu}{4\pi}\int_{h-\frac{L}{2}}^{h+\frac{L}{2}} I(z')g(z,z')dz' \qquad (4.22)$$

where

- $I(z')$ is the unknown axial current along the wire, and
- $g(z,z')$ is total Green function given as

$$g(z,z') = g_0(z,z') + R_{TM}g_i(z,z') \quad (4.23)$$

where

- $g_0(z,z')$ is the free space Green function, and $g_i(z,z')$ arises from MIT

$$g_0(z,z') = \frac{e^{-jk_0R_0}}{R_0} \qquad (4.24)$$

$$g_{\mathrm{i}}(z,z') = \frac{e^{-jk_{\mathrm{i}}R_{\mathrm{i}}}}{R_{\mathrm{i}}} \qquad (4.25)$$

where

- R_0 and R_i denote the distance from the source to the observation point, and
- R_{TM} is the reflection coefficient for the transverse magnetic polarization.

To obtain internal E field vector distribution through an exposed human body, current distribution along the antenna, needs to be evaluated. In case of wire antenna current distribution is governed by the Pocklington integro-differential equation. This can be achieved by applying continuity conditions for tangential field components on a perfectly conducting (PEC) wire surface (Figure 4.2.). The total electric field, composed from an incident and scattered field, respectively, disappears on the PEC wire [87]:

$$E_z^{inc} + E_z^{sct} = 0 \quad (4.26)$$

where

- E_z^{inc} is the tangential incident field, and
- E_z^{sct} is the scattered field.

Now, the Pocklington integro-differential equations for the unknown wire current I(z'):

$$E_z^{inc} = -\frac{j}{\omega 4\pi\varepsilon_0}\left[\frac{\partial^2}{\partial z^2} + k_0^2\right]\int_{h-\frac{L}{2}}^{h+\frac{L}{2}} I(z')g(z,z')dz' \quad (4.27)$$

Provided that current distribution along the wire is known (or assumed) Pocklington integro-differential equation is solved and the radiated field can be evaluated.

This chapter explained various simplifications for the modeling of a radiated wire antenna problem that would enable a closed analytical solution of the EM field described by Maxwell's equations. Potential methods for enabling the application of an analytical approach in solving the problem of quantifying interactions with EM waves were presented. Overall literature emphasizes that an analytical method is used when a problem requires an accurate solution, but can only be applied to very simple cases, and therefore, their use is somehow limited.

One of the simplest scenarios which can be used to assess human exposure to HF radiation is one where the human body is exposed to the EMF radiated by a thin wire antenna. A simple dipole antenna combined with a simple human body model is often used for quick dosimetry procedures, aiming to get a rapid estimation of the phenomena.

The chapter 5 and 6 are dedicated to internal EM dosimetry and thermal dosimetry. The aim of these chapters is to highlight the difference between analytical and numerical approaches to EMF, focusing on main assumptions and simplifications conducted using human body modeling.

5 Internal Electromagnetic dosimetry

To reach its intents, EM dosimetry relies on analytical, numerical or experimental techniques. Analytical methods are based on attempts to seek the theoretical solution of the field equations in general form. Numerical dosimetry makes use of computational techniques on digital computers to solve specific problems, while experimental dosimetry uses instrumentation and measurements to directly measure the dosimetric quantities.

Even if in general, analytical methods suffer from a few major intrinsic limitations (cannot easily accommodate complex environments, particular postures, different grounding patterns or internal body structure), they nevertheless are valuable because they often provide an insight into the qualitative nature of the coupling mechanisms. As for experimental dosimetry, analytical results are also useful as a check for numerical techniques.

Analytical methods give results that are applicable in a large number of applications and real-life use cases. In order to be applicable, the analytical solution must be verified by comparison with the results of numerical analysis and/or experimental measurements (if possible).

Compared to external fields, internal field quantification gives much better insight into the interaction between humans and EMFs. At higher RF frequencies, all known and anticipated EM interactions occur through a mechanism involving an electric field, since the magnetic permeability of almost all tissue is equal to that of free space. Therefore, the internal E field vector or its distribution through an exposed human body, at higher RF frequencies, fully describes field-tissue interactions. Additional information may be needed for full quantification, such as the frequency of exposure field.

Having in mind that the induced electric field is the main driver of biological processes that will take place in the human body as a result of exposure to EM radiation, establishing a mathematical relationship between incident and induced electric field is the next step in EM dosimetry procedure. Induced electric field inside the body has the same direction as the external field but is reduced in strength by a factor inversely proportional to the complex permittivity of tissue.

Although, early research in this field proposed the use of current density in tissue, or an internal electric field, a mass-normalized rate of energy absorption was introduced in the late 1960s.

Many researchers today rely on dose rate, which were formerly termed “absorbed power density” [37], and officially designated as SAR by the National Council on Radiation Protection and Measurements (NCRP). The first organization that adopted SAR as the fundamental dosimetry parameter was the American National Standards Institute (ANSI) [37].

SAR is defined as the rate of energy absorbed by or dissipated in human body unit mass, where two metrics are most often determined. The first metric is the whole body averaged SAR defines as the total EM power absorbed by a body divided by its mass. The second is the local SAR averaged over any cube inside the body with a tissue mass of 1 g (SAR-1 g) or 10 g (SAR-10 g). This value is usually reported independently of the exposed tissue. Since the current is induced, E and SAR are related by equitation (5.1) so it makes no difference which of the parameters is chosen for quantification.

$$SAR = \frac{d}{dt}\frac{dW}{dm} = \frac{d}{dt}\frac{dW}{\rho dV} = C\frac{dT}{dt} = \frac{\sigma E_{rms}^2}{\rho} = \frac{\sigma|E|^2}{2\rho} = \frac{J^2}{\sigma\rho} \qquad (5.1)$$

where

- W [J] is absorbed energy
- m [kg] is the mass of the tissue
- J [A/ m^2] is induced current density in tissue,
- ρ describes the mass density of human tissue,
- σ represents the tissue conductivity,
- E_{rms} the root mean square of the electric field strength,
- C is the specific heat capacity of tissue,
- T is the temperature, and
- t denotes time.

Whole-body averaged SAR is a single SAR value that represents the magnitude of spatially averaged SAR throughout an exposed biological object [37]. SAR averaged over a whole bode is given by [87]:

$$SAR_{WB} = \frac{1}{V}\int_V SAR_{surf}\,dV \qquad (5.2)$$

where

- V is the volume of the human body, and
- SAR_{surf} is the surface SAR value assumed to decrease exponentially through the human body, as follows:

$$SAR_{surf} = SAR_0 e^{-\frac{2x}{\delta}} \qquad (5.3)$$

where

- SAR_0 is the intensity of SAR at the surface as a function of depth x,
- x is depth, and
- δ is the is the penetration depth.

Evaluation of the maximum local SAR is especially important when a part of the human body is exposed to EM radiation from nearby sources. An example of such a situation, is the estimation of SAR distribution throughout a human head during the use of cellular telephones. The local SAR is the SAR that represents the magnitude of the SAR in a small portion of an exposed biological object [37].

$$SAR = \frac{\sigma |E|^2}{\rho_m} \qquad (5.4)$$

Both SAR types are averaged during a certain period of time and a tissue mass value over 1 g or 10 g is considered. SAR-10 g is obtained by averaging the maximum SAR of the points within the 10 g volume and this calculation is performed until it covers the whole sample volume. The same principle is applied for computing the SAR 1 g over 1 g volume covering the whole volume. The SAR (10 g or 1 g) value may be subsequently calculated considering the contribution of the smaller cube and the contribution of the cubical shell around it each with a predefined weighting coefficient using (5.5) [88]:

$$SAR(10\ g\ or\ 1g) = \frac{\sum_{v1} SAR_i m_i + \sum_{v2-v1} SAR_j m_j}{\sum_{v1} m_i + \sum_{v2-v1} m_j} \qquad (5.5)$$

where

- $m_i = \rho_i \Delta V$ is the mass of 10 g cell or 1 g cell
- $m_j = P_j \Delta V \frac{10-V1}{V2-V1}$ for 10 g cell and $m_j = P_j \Delta V \frac{1-V1}{V2-V1}$
- Index *i* refers to the lattice cells inside the inner cube, and
- index *j* to those around it.

According to ICNIRP for frequencies below 6 GHz and above 100 kHz, SAR should be used while for frequencies in the range 6–300 GHz absorbed power density (APD) should be used as the basic restriction for the human exposure to EMFs. APD is defined at the body surface, averaged over the tissue area of interest, A [89]

Absorbed power density for the general public should be restricted to 20 W/m2, averaged over 6 min and over a 4 cm2 area.

$$S_{ab} = \frac{1}{2A} \iint_A \Re(\vec{S}) d\vec{s} \qquad (5.6)$$

where

- $\vec{S} = \vec{E} x \vec{H}^*$ is the Poynting vector yields a direction of the electromagnetic wave propagation, and
- $d\vec{s}$ is variable vector normal to the integral area A

In addition to SAR and APD the metric transmitted power density to the skin surface or epithelial power density (TPD) is defined as [90]

$$TPD(x, y) = \frac{1}{2} \int \sigma(r) |E(r)|^2 dz \qquad (5.7)$$

where

- $|E(r)|$ is the peak value of the electric field at position r,
- σ is the conductivity of human tissue, and
- r is the direction perpendicular to the human body surface.

TPD corresponds to integrated SAR over the depth direction [90]. In the far-field region, wave propagation is spherical in nature and transmitted power density decays as $1/r^2$, where r is the distance from the antenna [84]. In guidelines and standard SAR_{10g} and Incident Power Density (IPD) are considered as metrics, but TPD at the surface is also evaluated in [90].

Biological effects and potential damage to humans due to the exposure to HF fields is caused through a temperature increase although safety standards are, up to now, expressed in terms of induced fields or SAR.

The amount of absorbed EM energy depends on incident field parameters (frequency, intensity polarization), zone of exposure (near field or far field), characteristics of the exposed object (size, geometry, dielectric permittivity and electric conductivity), and absorption or scattering effects of objects near the exposed body. Dielectric permittivity and electric conductivity are

discussed earlier, so a more detailed description of the geometry of the human body needs to be further elaborated.

Since the human body is very complex in the geometrical sense it is very difficult to form an exact analytical and/or experimental description of it. Different human body models have been developed in order to estimate SAR_{WB}. In the early beginning of dosimetric calculations homogeneous spheroidal and ellipsoidal models of humans were used [91]. Spheroid models can be useful in investigating the relationship between human height and a wavelength at resonance frequency [92]. Models such as spheres, cylinders, prolate spheroids, block models (cubical mathematical cells arranged in a shape like a human body), have been used to represent the human body energy absorbed during plane wave irradiation [93].

Later, sample geometry to describe the human body was used, such as a cylinder or a parallelepiped [39,90]. These planar models do not represent humans well, but analysis of these models has provided an important quantitative understanding of energy-absorption characteristics. When a plane wave is incident on a planar electrically lossy object, the wave transmitted into the object attenuates as it travels and transfers energy to the object. The more lossy the object, the more rapidly the wave attenuates.

High resolution, to the order of a millimeter or finer, and detailed numerical human models can be used today. The flat solid phantom provides easy handling and stable dielectric properties [94]. Realistic models have a rather high computational cost, while simplified ones are computationally much less expensive, but fail to ensure accurate results in most scenarios [95].

Based on the degree of complexity of the model's shape, the theoretical techniques used to calculate SAR, the human body model can be divided into three basic approaches [96]. The one-dimensional model is the simplest and particularly useful at HF frequencies where human body curvature can be neglected [96]. These simple models cannot predict human body resonance, occurring in finite sizes models.

The second group are two-dimensional models, basically single or multi-layered infinite cylindrical geometries that can simulate certain limbs, thighs or arms [96]. And the last group, three-dimensional models, include both idealized shapes and block models of biological cells [96]. Although the last group of models are the most complicated and can be solved only numerically, they offer the best estimates of average SAR and SAR distribution [96].

Analytical methods of EM dosimetry are usually applied to simple one-dimensional human body models. In this sense, in the rest of this chapter, the most significant characteristics of simple human body models that are more often used in the analyzed literature are presented.

5.1 Simple human body models

A planar and spherical model of the human body. Planar models are very simple, but their use is limited because they cannot represent the size and shape of the human body. Slightly more complex, and therefore more challenging to analyze, are spherical models that can better represent the human body (Figure 5.1.) [97].

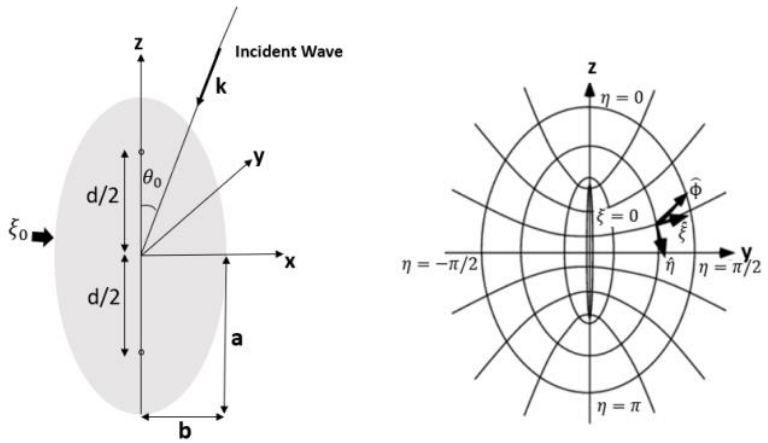

Figure 5.1. (Left) Prolate spheroid geometry; (right) and the spheroidal coordinate system [98]

The main advantages of spherical models are the simplicity of the technique [97]. Another advantage of using spherical shapes is the classical Mie series solution. Early information about whole-body average SAR was obtained by application of the classical Mei solution, where the internal electric field is obtained as an infinite series of spherical harmonics [97].

Spheres revealed that the SARs are very shape-dependent, and that they were incapable of accounting for different polarizations of incident plane-wave irradiation. The analysis of the prolate spheroidal models was extended to ellipsoidal, and layered cylindrical models that were relatively simple to use and provided excellent information on the whole-body-averaged SARs as a function of frequency for different polarizations of irradiation [97].

A parallelepiped model of the human body. A parallelepiped model (Figure 5.3.) is one of the simplified human body models mentioned in [79,95,99]. The parallelepiped human body

model dimensions are height of 180 cm, depth of 40cm, and width of 20 cm (W).

For parallelepiped human body model, average SAR can be expressed as

$$SAR_{WB} = \frac{1}{V}\int_V SAR_0 e^{-\frac{2x}{\delta}} dV = \frac{\delta}{2\Delta x} SAR_0 \left(1 - e^{-\frac{2\Delta x}{\delta}}\right) \quad (5.8)$$

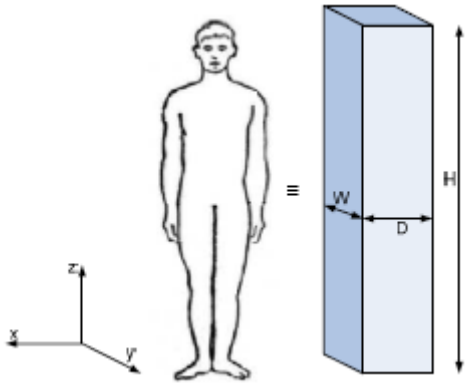

Figure 5.3. Parallelepiped human body model, dimensions: 180 cmx40 cmx20 cm (HxDxW) [95]

A cylindrical model of the human body. The cylindrical model of the human body presents the human body as a cylindrical scatterer of length L and radius a, placed vertically on an ideally conductive ground (Figure 5.4.), and these models are very useful at higher intermediate frequencies, i.e., just beyond resonance (between 400 MHz and 7 GHz [97]).

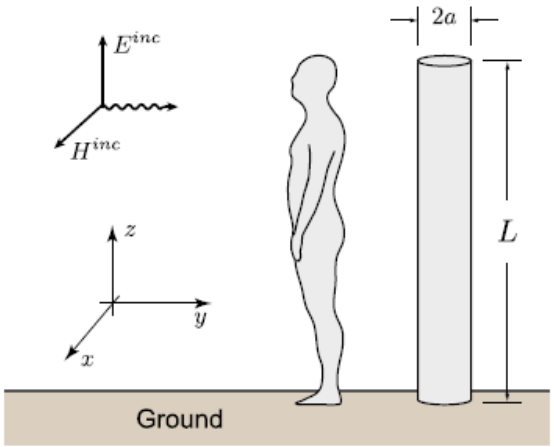

Figure 5.4. Cylindrical model of human body [100, 101]

Here difficulty lies in calculating the higher order Bessel functions of large complex argument that occur at higher frequencies. In this case, the tangential component of the electric field on the surface of the cylinder is the sum of the incident and scattered electric fields as described by the relation [101,102].

$$E_z^{tot}(a,z) = E_z^{inc}(a,z) + E_z^{sct}(a,z) \qquad (5.9)$$

Scattered field at the surface of the cylinder is given by the Pocklington integral equation [94]. Given that the human body is non-ideally conductive, losses in the cylinder can be added to the integral relation according to the equivalence theory, or through impedance loading as done by many authors [79,82-84]. After determining the current density, the incident electric field at any point in the cylinder *T(r,z)* can be determined using the following expression [103]:

$$E_z(r,z) = \frac{J_z(r,z)}{\sigma + j\omega\epsilon} \qquad (5.10)$$

If the antenna radiation is approximated by plane wave, the SAR can be calculated from the expression [104]:

$$SAR = \frac{\sigma}{\rho}\frac{\mu\omega}{\sqrt{\sigma^2+\omega^2\varepsilon^2}}\left(1+\gamma_{pw}\right)^2\frac{\left|E^{tot}\right|^2}{Z_0^2} \qquad (5.11)$$

where

- $\gamma_{pw} = \frac{2\left|\sqrt{\varepsilon'}\right|}{\left|\sqrt{\varepsilon'}+\sqrt{\varepsilon_0}\right|}$ is the reflection coefficient,
- ε' is the complex permittivity of the medium.

Initially, PEC cylinders were also used to observe the influence of people on indoor propagation. In conclusion, there is an analytical solution (long-wavelength approximation) that is valid at LFs and one at the higher intermediate frequencies (cylindrical solution) but not in the range near resonance, which is the region of greatest difficulty for calculating the SAR [97].

5.2 Phantoms

In contrast to sample analytical techniques, experimental and numerical dosimetry techniques can be used to assess internal fields for different sources and geometries. Phantoms simulating the human body or parts play a central role in radiation dosimetry. Phantoms are physical or computational. The most challenging task in designing physical phantoms are the uncertainty of the electrical properties measured by commercially available systems, temperature change and water evaporation [105]. Some example of already design and used physical phantoms can be find in [106,107]. Several teams [108] converted mathematical models and physical phantoms into voxel phantoms.

First computational phantoms were based upon mathematical expressions representing planes, and cylindrical, conical, elliptical, and spherical surfaces [91] – sample analytical models. Later,

more realistic replication of human anatomy was created by dividing human body model into small voxels (volume pixel). A voxel is a small volume element or cube of a desired tissue and with dimensions of a few millimeters on each side. A whole-human body human voxel model can consist of many million voxels. Each voxel is given appropriate dielectric properties according to which organ it belongs.

The first phantom, called NORMAN, was created in 1997 and consisted of 37 kinds of tissues with accuracy up to 2mm [109]. Later, in 2005, the same authors created first female phantom, NAOMI [110], and in 2007 three boys and two girls' children. Voxel models of whole-human body humans in various postures and of children, fetuses, and embryos have been developed by several laboratories [111-118]. Table 5.1. lists the basic characteristics of some anthropomorphic voxel phantoms of whole human body.

Table 5.1 Characteristics of some anthropomorphic voxel phantoms of whole human body

Name	**Gender**	**Age**	**Size [cm]**	**Weight [kg]**	**Imaging modality**
VIP-Man	Male	38 years	186	103	Photos
Meetman	Male	38 years	186	103	Photos, CT
RVH-female	Female	59 years	167	Unknown	CT
Golem	Male	38 years	176	69	CT
Donna	Female	40 years	176	79	CT
Baby	Female	8 weeks	57	4l.2	CT
Child	Female	7 years	115	21.7	CT
Norman	Male	Adult	170	70	IRM
UF-newborn	Female	6 days	*	3.83	CT
UF 2 month	Male	2 months	*	5.4	CT
Otoko	Male	Adult	170	65	CT

The external envelope of modified Zubal phantom is shown in Figure 5.7.

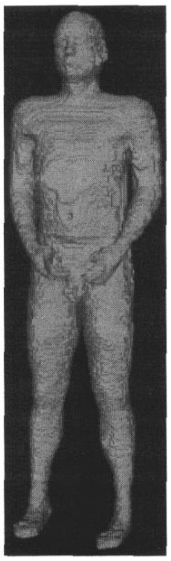

Figure 5.7. External envelope of the modified Zubal phantom [119]

Visible Photography-Man was developed at the Rensselaer Polytechnic Institute, New York and the only radiosensitive tissue not segmented in VIP-Man is the surface of the bones, since the spatial resolution required is too high for this structure. The Models for Simulation of Electromagnetic, Elastomechanic and Thermic Behavior of Man (MEETMAN) project was developed at the Institute of Biomedical Engineering at Karlsruhe University, in Germany and also consists of a very realistic anatomical mode1 of the human body. Reduced Visible Human (RVH) phantoms are used for research into intensity modulated radiotherapy (IMRT). The advantage Golem has over the Visible Human Project phantoms lies in the fact that its weight and size agree well with those of the Reference Man [120,121]. In Donna the number of segmented organs was fewer than for Golem, and the resolution is better in the transverse matrix compared to that of Golem.

Intrinsic disadvantage of voxel models is that they are usually based on the anatomy of a single man or woman [122], such as VoxelMan [120,121], MAX (Male Adult voXel) and FAX (Female Adult voXel) models [121]. Further on, they do not contain any spatial information at scales smaller than their native resolution and that they cannot be easily deformed to adopt different postures [122]. These problems can be overcome by adopting a Computer Aided Design (CAD) approach to develop models in which the organ and tissue boundaries are represented by parametric surfaces. Further on, the lack of anatomical detail and precision together with thermoregulatory mechanism, limits the applicability of these models to relatively gross thermal response.

First full-human body anatomical model, called Utah Anatomic Model [115], was created from a live person Magnetic Resonance Imaging (MRI) during 18h and 3 separated days. Authors in [123] developed a CAD-based human model which can easily move and rotate in any direction with 3-D CAD software and no limitation of their spatial resolution. The surfaces of the model can be readily deformed, but care must be taken for the joints of the human body to be correctly articulated. CAD models are usually segmented into voxel models at the required resolution before carrying out Finite-difference time-domain method (FDTD) calculations. The Baby and Child phantoms are among the rare pediatric phantoms described in the literature [124].

Norman, the phantom created by Dimbylow [113] is one of the only whole-human body phantoms created from MRI images, which has incidentally caused problems in segmentation of the bones. UF-newborn was created from CT images of a 6-day-old female cadaver imaged within 24 hours of death. It was created from CT images of a 6-month-old male cadaver imaged within 6 hours of death. Otoko is the standard adult Japanese male weighs 60 kg, and is 170 cm tall.

Over the years, experimental phantoms have been developed to understand coupling of EM fields to models of the biological systems. Although these models were relatively crude representations of the size and shape of the human body in beginning, experimental results show that calculations of the average SAR agree reasonably well with empirical values [91]. While most of these models do an excellent job of modelling the external shape of the exposed bodies, detailed modeling of the internal heterogeneities of the human body is very difficult and has been attempted only on a very limited scale and in a relatively crude manner [125]. Simple homogeneous models have, therefore, been used more often [126]. Numerical methods, e. g., the finite integration technique (FIT), can be used to precisely determine the effects of EM waves for a complex heterogeneous model such as a voxel model of a human body [61].

Studies show that analytical models in EM dosimetry can provide the satisfying level of accuracy under some conditions which makes them attractive to research. Besides simplicity and possibility for closed form solution, these models yield relatively precise results for electric field magnitude and SAR in regions of the human body with isotropic electrical behavior and when exposed area is approximately plane [61].

6 Thermal dosimetry

As described earlier, the main effect of exposure to HF fields is heating. In HF range the human body dimensions are comparable to external field wavelength and resonances become significant, so thermal effects are dominant. Better understanding of process that actually happens in biological tissues as a result of EM interaction is needed to obtain the increase of tissue temperature and to conclude if the radiation effects are hazard for humans or not. To obtain the desired temperature increase in HF frequency range, it is important to know the time of exposure. Since in human body skin is the largest living organ, temperature distribution in skin tissue is very important for medical application such as skin cancer, skin burns etc. [127].

By the definition, the occurrence of storing a larger amount of energy than the thermoregulatory capacity of the human body, is referred to as the thermal effect [101]. There are numerous models that can be used to describe the process of heat exchange, but the model proposed by Penne's is widely used, because of its simplicity and acceptable accuracy if no large thermally significant blood vessels are close to the analyzed heated region [128]. Solutions of Penne's bioheat equation (PBHE) were obtained in regions with Cartesian, cylindrical and spherical geometries. PBHE describes the energy balance between conductive heat transfer per tissue volume unit, heat loss due to perfusion, metabolism and energy absorption due to radiation. The PBHE has the following form [38, 129]:

$$\underbrace{\nabla(\lambda\nabla T)}_{heat\ flux} + \underbrace{W_b c_b (T_a - T)}_{perfusion\ rate} + \underbrace{Q_m}_{metabolism} + \underbrace{Q_{EM}}_{EM\ energy} = \rho_t c_t \frac{\partial T}{\partial t} \qquad (6.1)$$

where

- λ is the thermal conductivity [W/m°C],
- W_b is the volumetric perfusion rate [kg/m^3]
- T is the tissue temperature [°C],
- c_b is the specific heat of blood [J/kg°C],
- T_a is the arterial temperature [°C],
- Q_m is the power produced by metabolic process [W/m^3],
- Q_{EM} is the EM power deposition [W/m^3],
- ρ_t is tissue density [kg/m^3],

- c_t is the specific heat of tissue $[\mathrm{J}/kg℃]$, and
- t is the time [s]

Q_{EM} represents the resistive heat generated by the EM source and is expressed as [38]:

$$Q_{EM} = \frac{\sigma}{2}|E|^2 \qquad (6.2)$$

where

- σ is the electric conductivity [S/m] of the tissue, and
- E is the maximal value of the electric field induced inside the human body.

Dissipated power density Q_{EM} is directly related to SAR, as follows [101]:

$$Q_{EM} = \rho SAR \qquad (6.3)$$

PBHE equation was used in numerous studies to predict temperature changes in biological tissue [130-133]. Thermal tissue parameters (blood perfusion rate, the metabolic rate and the conductivity) are assumed to be time and temperature independent [134,135]. The rise of local temperature in tissue is consequence of oscillations in the molecules produced by absorbed EM energy [38], and if PBHE is stationary it is a linear equation in terms of temperature T.

To reach PBHE solution the BCs at the interface between tissue types with different electrical and dielectric properties, including the human body and ambient air needs to be define. Generally, BCs belong to one of three types: Dirichlet, Neumann or Robin.

Dirichlet BC related to unknown temperature field is [136];

$$T(\boldsymbol{x}, t) = \bar{T}(\boldsymbol{x}, t), \boldsymbol{x} \in \Gamma_m \qquad (6.4)$$

Neumann BC for the boundary heat flux is [133]:

$$q(\boldsymbol{x}, t) = \bar{q}(\boldsymbol{x}, t), \boldsymbol{x} \in \Gamma_q \qquad (6.5)$$

Convection or Robin BC is [97,133]:

$$q(\boldsymbol{x}, t) = -\lambda \frac{\partial T}{\partial n} = H(T_s - T_a)\,, \boldsymbol{x} \in \Gamma_c \qquad (6.6)$$

where

- q denotes the heat flux,
- n is the unit outward normal to the boundary Γ of the interesting domain,
- H is the convection coefficient,
- T_s is the temperature of the skin, and

- T_a denotes the temperature of the air.

Heat flux refers to the general heat flux and encompasses convection described by the heat transfer coefficient [137], directed to the internal normal. A positive value corresponds to a heat source, and negative value represent a heat sink. The expression $H(T_s - T_a)$ describes convective heat transfer with the surrounding environment. The value of H depends on the geometry and the ambient flow conditions.

As is the case with EM dosimetry, the PBHE can be solved both analytically and numerically. Traditionally, numerical methods are used when analytical solutions are not available, that is, analytical methods are preferred because they are simple and their effectiveness is less dependent on the dimensionality of the problem compared to numerical methods. The fact that the use of analytical methods significantly saves computer resources is one of the reasons for their application in some cases of hyperthermia in practice [131,138,139].

Furthermore, analytical methods can accurately reflect not only the actual physical feature of equations but also be used as standards to verify corresponding results obtained using numerical calculation [138,139]. The analytical solutions are very interested due to their exact estimation and lower cost in comparison with experiment and numerical calculations [140]. Introducing more than one region into a thermal model of the skin tissue leads to intractable analytical solutions, so numerical methods were used instead.

For simplicity, in most of the early studies on skin bioheat transfer, the human skin is modeled as a single layer. Built upon the single layer model [141-144], various multilayer skin models have been proposed: a two-layer skin model, which is composed of epidermis and subdermal tissue in most cases [145-148], a three-layer model, which is mostly composed of epidermis, dermis, and subcutaneous fat [149-153], and a four-layer model, which is composed of stratum corneum, epidermis, dermis, and subcutaneous fat [154-155].

A closed-form analytical solution of the PBHE is suitable for long run steady periodic temperature oscillation, but cannot satisfy the starting transient temperature response. Challenging task for numerical solution is frequency above 2 GHz, where the human body behaves like a large electrical structure. In such conditions, in order to reduce the dispersion error during modelling, several cells per wavelength must be modelled [156]. This implies the

use of computationally demanding simulations (depending on the chosen human body model and operating frequency).

Some of the numerical approaches used to solve PBHE in analyzed literature include the BEM [156], the FEM [156], the FDM [157], the FEM [158], the DRMBEM [159], the MCM [138, 160], the and the Meshless method [161,162].

Among numerical methods, the major drawback of the FDM appears to be its inability to effectively handle the solving of problems over arbitrarily shaped complex geometries because of interpolation difficulties between the boundaries and the interior points in order to develop finite difference expressions for nodes next to the boundaries. The FEM is widely used because it can compute complex shapes well, such as the human eye [153], but its main disadvantage is that it requires domain discretization which is time-consuming. The BEM involves the discretization of the boundary only, which is an important advantage over the FEM, but it has difficulty dealing with transient or nonhomogeneous problems which still need domain discretization. Fortunately, the DRMBEM can overcome this drawback by combining radial basis functions and the conventional BEM to transform domain integrals to the boundary integral. An alternative numerical method is the MCM, which differs from the classical numerical methods listed above because it is based on a random process approach and depends less on the dimension of the problem, providing an alternative way to deal with multidimensional problems.

New mathematical models for PBHE using the methodology of fractional calculus was constructed in [163] and then solved numerically. This approach is considered to be analytical-numerical hybrid method. Another analytical-numerical hybrid method is the Variational Iteration Method (VIM) [164]. Pure analytical methods include the Laplace transform method [128], a Method based on modified PBHE (MPBH) [133], a Method based on Bessel functions [166], the method based on Green's function [167], and Separation of Variables (SoV) [136].

The hybrid fractional derivatives method is based on introducing dimensionless quantities (6.7) into relation (6.1) transforming it into relation (6.8) [163]:

$$\tau = \frac{tc_bW_b}{\rho c}, \xi = x\sqrt{\frac{c_bW_b}{\lambda}}, \phi = \frac{Q_{EM}}{c_bW_bT_a}, \theta = (T - T_a)T_0^2 \qquad (6.7)$$

$$\frac{\partial\theta}{\partial\tau} = \phi - \theta + \frac{\partial^2\theta}{\partial\xi^2} \qquad (6.8)$$

where

- t presents time,
- c_b denotes specific heat of blood,
- W_b shows blood perfusion rate,
- ρ indicates density,
- c denotes specific heat,
- λ is the thermal conductivity,
- T is temperature distribution,
- Q_{EM} refers to an external heat source in skin tissue, and
- T_a states artillery temperature,

Imposed conditions before and after the use of dimensionless variables [163]:

$$T(z,0) -> T_a \text{ and } T(z,t)_{z\to\pm\infty} = 0 \qquad (6.9)$$

$$\theta(\xi,0) = 0, \theta(\xi,\tau)_{\xi\to\pm\infty} = 0, \theta(0,\tau) = 1 \qquad (6.10)$$

The development of the ordinary bioheat transfer equation into the fractional bioheat transfer equation by replacing the first order time derivative within the fractional order $\mu_1 \in [0,1]$ and $\mu_2 \in [0,1]$ as [163]:

$$\frac{\partial^{\mu_1}\theta}{\partial\tau^{\mu_1}} = \phi - \theta \qquad (6.11)$$

$$\frac{\partial^{\mu_2}\theta}{\partial\tau^{\mu_2}} = \phi - \theta + \frac{\partial^2\theta}{\partial\xi^2} \qquad (6.12)$$

where

- $\frac{\partial^{\mu_1}\theta}{\partial\tau^{\mu_1}}$ is the well-known fractional derivative namely Atangana–Baleanu operator, and
- $\frac{\partial^{\mu_2}\theta}{\partial\tau^{\mu_2}}$ is the fractional derivative namely Caputo–Fabrizio operator.

When the relations for operators (6.11) and (6.12) are transformed into the frequency domain by applying the Laplace transformation, higher-order inhomogeneous differential relations will be obtained that can be solved in a systematic way by applying the concept of infinite series [163]. By applying Laplace's inverse transformation, temperature distribution from Penne's bioheat transfer model can be determined.

Variational Iteration Method is a semi-numerical method that is applied directly, without linearization, perturbations or the introduction of restrictive assumptions [164]. In this sense,

the nonlinear partial differential equation (6.37) is observed in which $Lf(x,y,t)$ and $Rf(x,y,t)$ are linear operators, $Nf(x,y,t)$ is a nonlinear operator and $g(x,y,t)$ is a heterogeneous term. By using the correlation function, successive approximations are established by determining the Lagranian multiplier by variational theory. The first Lagrangian multiplier is determined by integration by parts [164].

$$Lf(x,y,t) + Rf(x,y,t) + Nf(x,y,t) = g(x,y,t) \qquad (6.13)$$

The application of this method to PBE starts from a dimensionless relation for the evaluation of temperature in the tissue, together with associated BCs:

$$\left(1 + \tau\frac{\partial}{\partial t}\right)\frac{\partial\theta}{\partial t} = \nabla^2\theta - p_f\theta + \left(1 + \tau\frac{\partial}{\partial t}\right)G \quad (6.14)$$

$$\theta(0,y,t) = \theta^* e^{(\omega t + iby)}, G = g^* e^{(\omega t + iby)} \quad (6.15)$$

where

- τ is relaxation time,
- $\theta = \frac{T - T_a}{L^2/k}$,
- T is tissue temperature
- T_a is arterial blood temperature,
- $p_f = \frac{\omega_b C_b L^2}{\lambda}$
- L is tissue length,
- ω_b is perfusion due to blood flow,
- C_b is the specific heat capacity of blood,
- $G = \frac{Q}{Q_0}$,
- Q is absorbed power density,
- θ^* is the amplitude of the function θ,
- g^* is the amplitude of the function G,
- ω s the complex time constant, and
- b is the y-direction wave number.

Applying VIM to relation (6.14), i.e. constructing a correlation function in the x direction, the iteration formula in the x direction is determined, and using initial conditions, the desired number of iterations of the solution can be determined to the desired levels of accuracy [164].

Given that the focus of the paper is on analytical methods, they will be described in more detail.

6.1 Analytical methods

The problem geometry is shown in Figure 6.1..

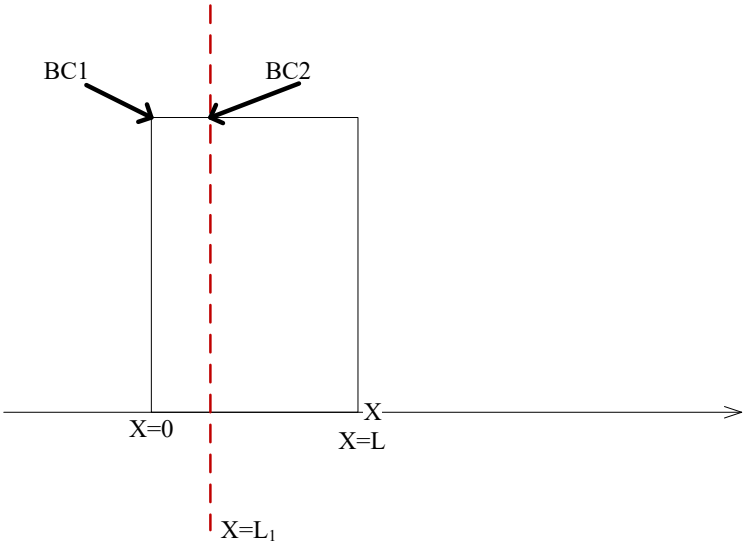

Figure 6.1. The geometry of the problem

The Laplace Transform method is one of the most used ways to solve the bioheat equation. The use of the Laplace transform technique maps the transient problem into the steady one. Although the application of the Laplace transform for the removal of the partial derivative is a relatively straightforward matter, the inversion of the transformed solution generally is rather involved unless the inversion is available in the standard Laplace transform tables. Before explanation of Laplace transformation in solving the PBHE, the definition of (direct) and inverse Laplace transform is introduced.

The Laplace transform (L) of function f(t) denoted by F(s), s being the complex variable is defined as [136]:

$$F(s) = \bar{f}(s) = L\{f(t); s\} = \int_0^\infty e^{-st} f(t)dt; t \in R^+ \qquad (6.16)$$

Inverse Laplace transform (L^{-1}) of F(s) is defined as [136]:

$$f(t) = \{F(s); t\} = \frac{1}{2\pi i}\int_{\gamma-i\infty}^{\gamma+i\infty} e^{st} F(s)ds; t \in R^+, \gamma = R(s) \qquad (6.17)$$

where

- s is the Laplace transform variable,
- $i \equiv \sqrt{-1}$, and
- γ is a positive number

Because of the geometrical features of the skin, the heat exchange in space domain is assumed to be one-dimensional. Different time-dependent surface heat flux is applied on skin surface, namely, continuous, periodic and ramp type [165] or sinusoidal heat flux [128].

The solution for one-dimensional PBHE for the transient problem, starts by observing PBHE (6.18) and oscillatory heat flux BC (6.19) [128]:

$$\lambda \frac{\partial^2 T}{\partial x^2} = W_b c_b (T - T_a) + \rho_t c_t \frac{\partial T}{\partial t} \qquad (6.18)$$

$$-\lambda \left. \frac{\partial T}{\partial x} \right|_{x=0} = q_0 e^{i\omega t} \qquad (6.19)$$

where

- q_0 is the heat flux on the skin surface, and
- ω is the heating frequency.

Introducing the dimensionless variables (6.20), (6.18) is transformed to (6.21) and (6.19) to (6.22):

$$z \equiv \omega t, \alpha \equiv \frac{\lambda}{\rho_t c_t}, X \equiv \sqrt{\frac{\omega}{\alpha}} x, c_1 \equiv \frac{W_b c_b}{\rho_t c_t \omega}, \theta \equiv \frac{\lambda (T - T_a)}{q_0} \sqrt{\frac{\omega}{\alpha}} \qquad (6.20)$$

$$\frac{\partial \theta}{\partial z} + c_1 \theta = \frac{\partial^2 \theta}{\partial X^2} \qquad (6.21)$$

$$\left. \frac{\partial \theta}{\partial X} \right|_{X=0} = -e^{iz} \qquad (6.22)$$

Laplace transform of (6.21) gives (6.23), and general solution is given in (6.24):

$$\frac{\partial^2 \phi}{\partial X^2} - (s + c_1)\phi = 0 \qquad (6.23)$$

$$\phi = c_2 e^{-\sqrt{s + c_1} X} \qquad (6.24)$$

The Laplace transform of (6.22) is (6.25), and obtained value becomes (6.26)

$$\left. \frac{\partial \phi}{\partial X} \right|_{X=0} = -\frac{1}{s - i} \qquad (6.25)$$

$$c_2 = \frac{1}{(s-i)\sqrt{s+c_1}} \qquad (6.26)$$

After inserting c_2 in (6.24) and taking Inverse Laplace Transform, the temperature response of skin can be obtained:

$$\phi = \frac{e^{-\sqrt{s+c_1}X}}{(s-i)\sqrt{s+c_1}} \qquad (6.27)$$

$$\theta = \frac{e^{iz}}{2\sqrt{c_1+i}}\left\{e^{-\sqrt{c_1+i}X}erfc\left[\frac{X}{2\sqrt{z}} - \sqrt{c_1+iz}\right] - e^{\sqrt{c_1+i}X}erfc\left[\frac{X}{2\sqrt{z}} + \sqrt{c_1+iz}\right]\right\} \qquad (6.28)$$

$$\theta|_{X=0} = \frac{e^{iz}}{\sqrt{c_1+i}}erf\left[\sqrt{c_1+iz}\right] \qquad (6.29)$$

Finally, the solution of one-dimensional transient bioheat transfer equation with the periodic heating at the surface of living tissue is given by [128]:

$$T = T_a + \frac{q_0}{2\lambda}\left(\sqrt{\frac{\alpha}{(c_1+i)\omega}}e^{i\omega t}\right)\begin{Bmatrix} e^{-\sqrt{\frac{(c_1+i)\omega}{\alpha}}x}erfc\left[\frac{x}{\sqrt{4\alpha t}} - \sqrt{(c_1+i)\omega t}\right] \\ -e^{\sqrt{\frac{(c_1+i)\omega}{\alpha}}x}erfc\left[\frac{x}{\sqrt{4\alpha t}} + \sqrt{(c_1+i)\omega t}\right] \end{Bmatrix} \qquad (6.30)$$

Temperature elevation in the analytical model due to 60 GHz EM wave exposure for the three-layer model and one-layer model that consists of skin only is show in Figure 6.2.

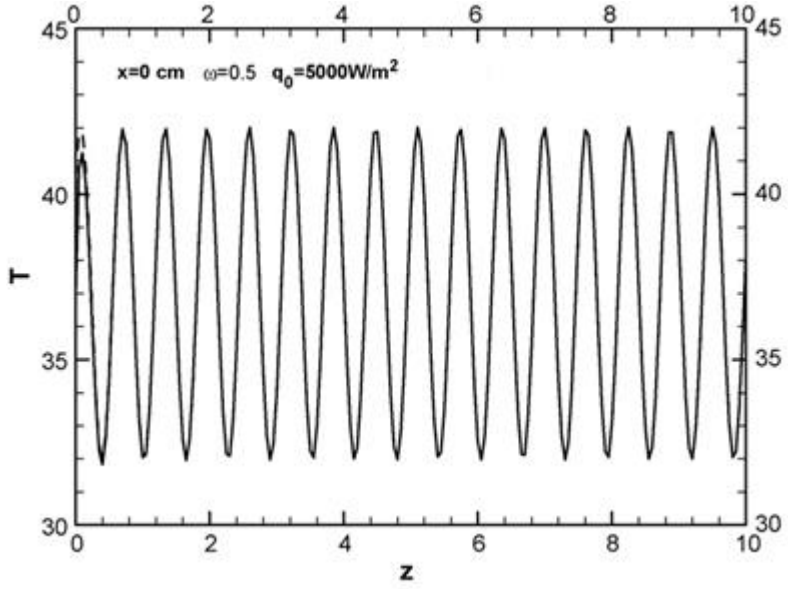

Figure 6.2. Tissue temperature vs tissue depth for Laplace transform method [128]

Detailed explanation about solution for 1D Penne's equation for an n-layer skin model excited by a plane wave directed in the z-axis direction can be find in [128].

A Method based on modified PBE is based on introducing temperature-dependent variability into tissue perfusion into Penne's basic equation. Temperature at x in the tissue and at time t is described by the equation [133]:

$$\frac{\partial T}{\partial t} = \lambda \frac{\partial^2 T}{\partial z^2} + \left[\omega_0 + \omega_1 \frac{T - T_a}{T_a}\right](T_a - \mathrm{T}) = 0 \qquad (6.31)$$

where

- ω_0 is the temperature-independent (basal) perfusion component, and
- ω_1 is the temperature-dependent (vasodilation and angiogenesis) perfusion component.

The analytical solution of the MPBH equation is based on two assumptions (6.32) and (6.33) [133]:

$$T_a = \text{constant} \qquad (6.32)$$

$$\frac{\partial T}{\partial t} = 0 \qquad (6.33)$$

Multiplying both sides of (6.34) by $\frac{dT}{dz}$, we obtained (6.35)

$$\frac{\partial^2 T}{\partial z^2} = \frac{\omega_1}{\lambda T_a} T^2 + \frac{\omega_0 - 2\omega_1}{\lambda} T + \frac{T_a(\omega_1 - \omega_0)}{\lambda} \qquad (6.34)$$

$$\left(\frac{dT}{dz}\right)^2 = 4\beta T^3 + 4\gamma T^2 + 4\delta T + \varepsilon = R(T) \qquad (6.35)$$

$$\beta = \frac{\omega_1}{6\lambda T_a}, \gamma = \frac{\omega_0 - 2\omega_1}{6\lambda}, \delta = \frac{T_a(\omega_1 - \omega_0)}{2\lambda} \qquad (6.36)$$

where

- ε is a constant of integration.

The solution to this equation (6.35) is:

$$T(x) = T_0 + \frac{R\prime(T_0)}{4[\wp(x; g_2, g_3) - \frac{1}{24} R''(T_0)]} \qquad (6.37)$$

where

- T_0 is the simple nonnegative root of R(T) and the prime denotes differentiation with respect to T.
- $\wp(x; g_2, g_3)$ is Weierstrass' eliptic function
- $g_2 = -4\beta\delta + 3\gamma^2$ and $g_3 = 2\beta\delta - \gamma^3$ are invariants of Weierstrass' eliptic function

The temperature along the distance x (in mm) from the heat source when $\omega_0 = 4.7619x10^{-4}s^{-1}, T_a = 37℃$ and $\omega_1 = 6.449x10^{-3}s^{-1}$ is shown in Figure 6.3..

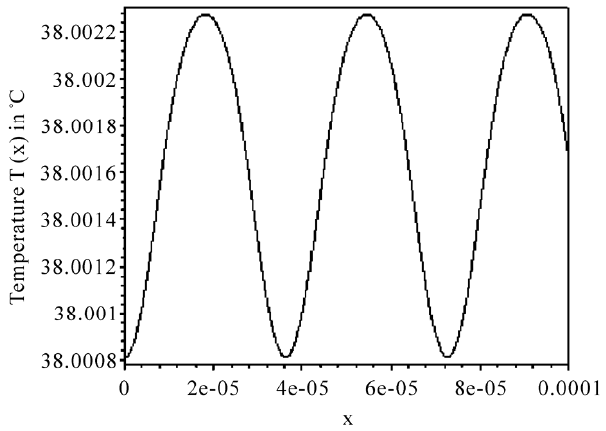

Figure 6.3. Tissue temperature vs tissue depth for Modified PBE [133]

Bessel functions under certain conditions, describe the PBE solution. To obtain the solution represented by Bessel functions, we start from the PBE equation in cylindrical coordinates (r, θ, z) [166]:

$$\rho c \frac{\partial T}{\partial t} = \frac{1}{r}\lambda \frac{\partial^2 T}{\partial r^2} + \frac{1}{r^2}\lambda \frac{\partial T}{\partial r} + \lambda \frac{\partial^2 T}{\partial z^2} + \frac{1}{r^2}\rho_b c_b \omega_b (T_a - T) + \frac{1}{r^2} Q_m \quad (6.38)$$

For one-dimensional steady-state case only the radial direction 'r' is taken [166]

$$r\frac{\partial^2 T}{\partial r^2} + \frac{\rho_b c_b \omega_b}{\lambda}(T_a - T) + \frac{Q_m}{\lambda} = 0 \quad (6.39)$$

Using BCs:

$$r = 0 \frac{dT}{dr} = 0 \quad (6.40)$$

$$r = R - \lambda \frac{dT}{dr} = h_A (T - T_\infty) \quad (6.41)$$

where

- R is the radius of concerned tissue;
- h_A is the coefficient of heat transfer on the surface of the tissue,
- T_∞ is atmospheric temperature, and
- $T_a =$ temperature of blood upon entering tissue via arterial.

After non-dimensionalization of the equation (6.39), and minor mathematical manipulation (6.39) becomes (6.42) which is Modified Bessel's equitation of the form (6.43) [166]:

$$r^{*2}\frac{d^2\varphi}{dr^{*2}} + r^*\frac{d\varphi}{dr^*} - Vr^*\varphi = 0 \qquad (6.42)$$

$$x^2\frac{d^2y}{dx^2} + x\frac{dy}{dx} - (x^2 + p^2)y = 0 \quad (6.43)$$

where

- $r^* = \frac{r}{R}$.
- $V = \frac{R^2}{\lambda}$
- $x = r^*$
- $\beta = \sqrt{V}$
- p=0

The solution of (6.43) is (6.44), and of (6.42) is (6.45) [166]:

$$y = AI_p(\beta x) + BK_p(\beta x) \qquad (6.44)$$

$$T = T_\infty + (T_a - T_\infty)\left[\frac{U}{V} - \frac{1}{V}\left\{\frac{h_A * J_0(\sqrt{V}r*)}{h_A * J_0(\sqrt{V}r*) + \sqrt{V}J_1(\sqrt{V}r*)}\right\}\right] \quad (6.45)$$

where

- $U = \frac{R^2}{\lambda} + \frac{Q_m R^2}{\lambda(T_a - T_\infty)}$,
- J_0 is the Bessel function of the zero order first kind, and
- J_1 is the Bessel function of the first order first kind.

The method based on Green's function is suitable for determining temperature distribution for different time-space profiles of the heat source, since it does not depend on it. The expression for that temperature is [140]:

$$T(x, y) = T_0(x) + W(x, t)e^{\left(-\frac{\omega_b \rho_b c_b}{\rho c}t\right)} \quad (6.46)$$

where

- $T_0(x)$ is the initial temperature field for the basal state of biological bodies obtained through solving the following equations [142]

$$\begin{cases} k\dfrac{d^2T_0(x)}{dx} + \omega_b\rho_b c_b[T_a - T_0(x)] + Q_m = 0 \\ T_0(x) = T_c, x = L \\ -k\dfrac{d\,T_0(x)}{dx} = h_0[T_{air} - T_0(x)], x = 0 \end{cases} \quad (6.47)$$

- $W(x,t)$ is an auxiliary function expressed as the sum of two Green's functions.

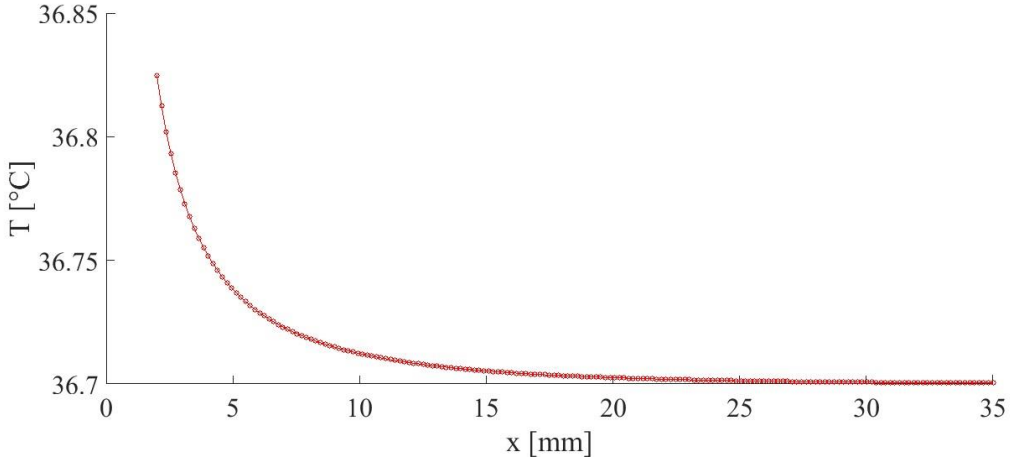

Figure 6.4. Tissue temperature vs tissue depth for the method based on Green's function

The method based on Separation of Variables. The basic concepts of SoV will be shown for a transient, boundary value problem of heat conduction for a 1-D slab (i.e., plane wall) over the domain $0 \leq x \leq L$ [136]. Initially the slab is at a temperature $T = F(x)$, and for times $t > 0$, the boundary surface at $x = 0$ is kept insulated while the boundary at $x = L$ dissipates heat by convection with a heat transfer coefficient h into a fluid of temperature T_∞. There is no heat generation in the medium. The mathematical formulation of this problem is given as:

$$\frac{\partial^2 T(x,t)}{\partial x^2} = \frac{1}{\alpha}\frac{\partial T(x,t)}{\partial t} \qquad 0 < x < L, t > 0 \quad (6.48)$$

$$BC1: \left.\frac{\partial T}{\partial x}\right|_{x=0} = 0 \quad (6.49)$$

$$BC2: -\lambda \left.\frac{\partial T}{\partial x}\right|_{x=L} = h[T|_{x=L} - T_\infty] \quad (6.50)$$

$$IC: T(x, t = 0) = F(x) \quad (6.51)$$

The requirement of a homogeneous Partial Differential Equation (PDE) is satisfied by equation (6.45), but the requirement for a transient problem of all homogeneous BCs is not satisfied, as the BC at $x = L$ contains the nonhomogeneous term T_∞. This type of nonhomogeneous

convective BC is readily removed by linearly shifting the temperature scale, namely defining a new temperature:

$$\theta(x,t) = T(x,t) - T_\infty \quad (6.52)$$

Now the problem in terms of the new dependent variable $\theta(x,t)$ is given as:

$$\frac{\partial^2\theta(x,t)}{\partial x^2} = \frac{1}{\alpha}\frac{\partial\theta(x,t)}{\partial t} \qquad 0 < x < L, t > 0 \quad (6.53)$$

$$BC1\text{: } \left.\frac{\partial\theta}{\partial x}\right|_{x=0} = 0 \qquad (6.54)$$

$$BC2\text{: } -\lambda \left.\frac{\partial\theta}{\partial x}\right|_{x=L} = h\theta|_{x=L} \qquad (6.55)$$

$$IC\text{: } \theta(x,t=0) = F(x) - T_\infty = G(x) \quad (6.56)$$

With this temperature shift, all requirements for SoV are assuming a separation of $\theta(x,t)$ into space-dependent and time-dependent functions of a single variable each, namely [136],

$$\theta(x,t) = X(x)\Gamma(t) \quad (6.57)$$

We now substitute equation (6.53) into (6.49) and introduce a separation constant, and sign of the separation constant is chosen to force the boundary value problem in the homogenous x dimension.

$$\frac{1}{X}\frac{d^2X}{dx^2} = \frac{1}{\alpha\Gamma}\frac{d\Gamma}{dt} = -\lambda^2 \qquad (6.58)$$

Using (6.54)

$$\frac{d^2X}{dx^2} + \lambda^2 X = 0 \qquad (6.59)$$

$$BC1\text{: } \left.\frac{dX}{\partial x}\right|_{x=0} = 0 \qquad (6.60)$$

$$BC2\text{: } -\lambda \left.\frac{\partial X}{dx}\right|_{x=L} = hX|_{x=L} \qquad (6.61)$$

$$\frac{d\Gamma}{dt} + \alpha\lambda^2\Gamma = 0 \qquad (6.62)$$

The homogeneous solution is

$$X(x) = C_1\, cos(\lambda x) + C_2 sin\,(\lambda x) \qquad (6.63)$$

According to BC1 $C_2 = 0$, and according to BC2 (6.59) can be rearranged to transcendental equation (6.60), where roots λ_n are the eigenvalues

$$-\lambda[-C_1\,\lambda sin(\lambda L)] = hC_1 cos\,(\lambda L) \qquad (6.64)$$

$$\lambda_n\, tan(\lambda_n L) = \frac{h}{k} \rightarrow\ \lambda_n, for\ n = 1,2,3,\ldots \qquad (6.65)$$

When solving equation (6.59), it is useful to multiple by L and define a new parameter $\beta_n = L\lambda_n$, yielding the transcendental equation:

$$X_n(x)=C_n cos(\lambda_n x) \qquad (6.66)$$

$$\beta_n \, tan(\beta_n) = \frac{hL}{k} = Bi \rightarrow \beta_n, for\ n = 1,2,3, \ldots \qquad (6.67)$$

As before, after solving the boundary value problem corresponding to the homogeneous dimension, we now turn to the nonhomogeneous dimension, equation. This ODE yields the solution

$$\Gamma(t) = C_3 e^{-\alpha\lambda^2 t} \qquad (6.68)$$

Equations (6.60) and (6.62) are now combined, introducing a new constant $C_n = C_1 C_3$, to produce a solution of the original PDE of the form (6.64). and constructing general solution

$$\theta_n(x,t) = C_n cos\ (\lambda_n x) e^{-\alpha\lambda^2 t} \qquad (6.69)$$

$$\theta(x,t) = \sum_{n=1}^{\infty} C_n cos\ (\lambda_n x) e^{-\alpha\lambda^2 t} \qquad (6.70)$$

Applying the initial condition, a Fourier series expansion of $G(x)$ in terms of an orthogonal function over the interval $0 \leq x \leq L$.

$$G(x) = \sum_{n=1}^{\infty} C_n \, cos(\lambda_n x) \qquad (6.71)$$

Multiplying both sides by the orthogonal function for an arbitrary eigenvalue, say $\cos(\lambda_m x)$, and integrating from 0 to *L*

$$C_n = \frac{\int_{x=0}^{L} \mathrm{G(x)cos}\ (\lambda_n \mathrm{x})\mathrm{dx}}{\int_{x=0}^{L} \mathrm{cos}^2\ (\lambda_n \mathrm{x})\mathrm{dx}} = \frac{\int_{x=0}^{L} \mathrm{G(x)cos}\ (\lambda_n \mathrm{x})\mathrm{dx}}{N(\lambda_n)} \qquad (6.72)$$

where $N(\lambda_n)$ is the norm of the eigenfunction and is dependent on the specific nature of the eigenvalues, *T(x,t)*

$$T(x,t) = \sum_{n=1}^{\infty} C_n \mathrm{cos}\ (\lambda_n \mathrm{x}) \mathrm{e}^{-\alpha\lambda^2 t} + T_\infty \qquad (6.73)$$

$$T(x,t) = \sum_{n=1}^{\infty} \left[\frac{\mathrm{cos}\ (\lambda_n \mathrm{x}) \mathrm{e}^{-\alpha\lambda^2 t}}{N(\lambda_n)} \int_{x'=0}^{L} G(x') \mathrm{cos}\ (\lambda_n \mathrm{x}') \mathrm{dx}' \right] + T_\infty \qquad (6.74)$$

Prediction of heat transport has long been carried out by both analytical and numerical methods. Although analytical solutions fail when dealing with complex geometries or nonlinearities, they provide the tools for numerical code testing and also for performing a valuable sensitivity analysis of the parameters involved in a problem. To simplify the mathematical model, some assumptions must be made, such as: the skin tissue is homogeneous and isotropic, the skin tissue properties are independent of skin temperature, heat generated by metabolism is constant, blood perfusion rate is uniform spatially and temporally and independent of tissue temperature, and arterial blood temperature is constant.

Even if the solution method is the author's choice, the application of some methods requires the fulfillment of certain conditions, and the choice of method itself depends on the chosen human body model and thermal properties of exposed body model.

7 Summary

Analytical and numerical techniques can be used to determine the electromagnetic-thermal response of a human body exposed to HF radiation. The focus of this paper is the analysis of the analytical methods described so far together with circumstances in which they can be applied, and the simplifications that were introduced so that the problem could be solved in a closed form. Analytical techniques are so-called because, in contrast to numerical techniques, they consist of a specific solution to Maxwell's equations that is not based on a direct numerical solution and does not require the inversion of large matrices.

This work gives an overview of the analytical models used in the electromagnetic-thermal dosimetry of simple wire antennas. Starting from the source of radiation, through the medium, and all the way to the model of the human body, various simplifications have been proposed in the literature.

Even if radiation source modeling is not included in dosimetry, it is mostly part of the problem being solved. Regarding the field source, a plane wave as an incident field is adopted in a majority of papers, while in others, an elementary dipole is considered. When propagating through a medium with losses, in an environment that is not isolated from the influence of the earth, in order to ensure a solution in a closed form, an approximation of the reflection coefficient, must be introduced. In the analyzed literature, the most common use of the MIT reflection coefficient is suggested. The human body is modeled simply, as a sphere, parallelepiped, or cylinder, thus providing the conditions for dosimetry of the internal field.

Future work in the spectrum of analytical methods should be expanded to include those that are accurate enough to be used in the upcoming 5G systems. If the accuracy of such a method is good enough, and possibility for closed form solution exist, it will enable quick determination of dosimetric quantities. In this sense, the choice of highly simplified geometrics is essential due to the necessity of characterizing a structure resembling the human body and/or parts of it and having at the same time a closed form of the wave equation. Although the analytical solutions do not provide detailed dosimetry information for actual human bodies, they contribute to qualitative analyses. And analytical methods should be compared to numerical and or experimental and simulation models to overcome the possible drawbacks related to their lower accuracy.

With regard to the upcoming implementation of 5G systems, and the fear of the potential impact of these systems on the health of primarily people, and then animals, the importance of electromagnetic-thermal dosimetry is very great in this case. Of particular importance is the frequency range of 3 GHz, since a lot of systems already work in this band, and that it was the first choice in America and some countries in Europe.

In some situations, such as the rapid implementation of antenna systems is of great importance, so the time for conducting this analysis is limited. The simplicity of this approach is also very important in the conditions of complex antenna systems. In addition to the stated application of these solutions, they will offer a saving of computing resources, compared to numerical methods. Although many studies have been carried out to date, their technical limitations prevent applicability in special cases of use.

Besides the rapid implementation of antenna systems, analytical methods are particularly useful to test numerical codes, identify the structure resonant frequencies that represent conditions of maximum power deposition inside the human body, evaluate the effects of the spread of dielectric and geometric parameters, commonly inferred from literature, and can be used to select parameters of greater influence on SAR distribution. Because of their importance and widespread usability analytical methods are very important topic for in the research of EM dosimetry, which is the fourth conclusion of our study.

References

1. T.H. Hubing, “Survey of Numerical Electromagnetic Modelling Techniques”, Report. TR91-1-001.3, 1991.
2. N. Siauve, et al., “Electromagnetic fields and human body: a new challenge for the electromagnetic field computation,” C*OMPEL: The International Journal for Computation and Mathematics in Electrical and Electronic Engineering, Emerald*, vol. 22, no 3, pp. 457-469, 2013.
3. A.A. Salih, et al., “Evolution of Mobile Wireless Communication to 5G Revolution,” *Technology Reports of Kansai University*, vol. 62, no 05, pp. 2139-2151, 2020.
4. N. Bhandari, et al., “Evolution of Cellular Network: From 1G to 5G,” *International Journal of Engineering and Techniques*, vol. 3, no 5, pp. 98-105, 2017.
5. L.O. Afolabi, et al., “Evolution of Wireless Networks Technologies, History and Emerging Technology of 5G Wireless Network: A Review,” *J Telecommun Syst Manage*, vol. 7, pp. 176-181, 2018.
6. C.R. Vignesh, “Overview on Generations of Network: 1G, 2G, 3G, 4G, 5G,” *International Journal for research in emerging science and technology*, vol. 3, pp. 214-220, 2016.
7. M.M. Mir, S.Kumar, “Evolution of Mobile Wireless Technology from 0G to 5G,” *International Journal of Computer Science and Information Technologies*, vol. 6, no 3, pp. 2545-2551, 2015.
8. S. Mondal, et al., “A Survey on Evolution of Wireless Generations 0G to 7G,” *International Journal of Advance Research in Science and Engineering*, vol. 1, pp. 5-10, 2015.
9. M. Cakmak, Z. Albayrak, “A Review: Mobile Communication Past, Present and Future,” *In Proc. of the International Conference on Advanced Technologies, Computer Engineering and Science*, Safranbolu, Turkey, May 11-13, 2018, pp. 141-145.
10. W. Scharnhorst, et al., “Life cycle assessment of second generation (2G) and third generation (3G) mobile phone networks,” *Environment International*, vol. 32, pp. 656–675, 2006.
11. A.U. Gawas, “An Overview on Evolution of Mobile Wireless Communication Networks: 1G-6G,” *International Journal on Recent and Innovation Trends in Computing and Communication*, vol. 3, no 5, pp. 3130-3133, 2015.
12. M. Jaloun, Z. Guennoun, “Wireless Mobile Evolution to 4G Network,” *Wireless Sensor Network*, vol. 2, pp. 309-317, 2010.
13. J. Agrawal, et al., “Evolution of Mobile Communication Network: from 1G to 4G,” *International Journal of Multidisciplinary and Current Research*, vol. 3, pp. 1-4, 2015.
14. S. Saha, Y.C. Joshi, “4G communication technology-evolution and impact on business and economy in India,” *Amity Journal of Management*, vol. 6, no 2, pp. 30-37, 2018.
15. K. Singh, 4G Wireless Network Revolution, *IJCRT*, vol. 1, no 3, pp. 1-5, 2013.
16. J.R. Churi, et al., “Evolution of Networks (2G-5G)”, *In Proc. of the International Conference on Advances in Communication and Computing Technologies*, Aug. 9-11, Kochi, India, Aug. 9-11, 2012, 2349-784X.
17. R. Yusoff, et al, “Overview of Security Approaches in 4G LTE Network,” *In Proc. of the International Conference on Advanced Science, Engineering and Technology (ICASET)*, Dec. 21-22, Seberang Jaya, Penang, Malaysia, 2015.
18. A.A. Almazroi, “Performance analysis of 4G broadband cellular networks,” *International Journal of Advanced and Applied Sciences*, vol. 5, no 9, pp. 12-17, 2018.
19. P. Pawlak, et al. “On Measuring Electromagnetic Fields in 5G Technology,” *IEEE Access*, vol. 7, pp. 29826-29835, 2019.
20. K. Chaer, et al. “Blockchain for 5G: Opportunities and Challenges,” 2019 IEEE Globecom Workshops (GC Workshops), vol. 1-6, 2019.
21. M.S. Morelli, et al. “Numerical Analysis of Electromagnetic Field Exposure from 5G Mobile

Communications at 28 GHZ in Adults and Children Users for Real-World Exposure Scenarios," *Int J Environ Res Public Health*, vol. 18, no 3, pp. 1073-1079, 2021.
22. M. Celaya-Echarri, et al. "From 2G to 5G Spatial Modelling of Personal RF-EMF Exposure Within Urban Public Trams," *IEEE Access*, vol. 8, pp. 100930-100947, 2020.
23. M. Zhabadov, et al. "Millimetre-wave interactions with the human body: State of knowledge and recent advances," *International Journal of Microwave and Wireless Technologies*, vol. 3, no 2, pp. 237-247, 2011.
24. M. Bonato, et al. "Stochastic Dosimetry Assessment of the Human RF-EMF Exposure to 3D Beamforming Antennas in indoor 5G Networks," *Appl. Sci*., vol. 11, pp. 1751, 2021.
25. C.C. Johnson, A.W. Guy, "Nonionizing electromagnetic wave effects in biological materials and systems," *Proc. IEEE*, vol. 60, pp. 692–718, 1972.
26. S.M. Michaelson, "Human exposure to nonionizing radiant energy- Potential hazards and safety standards," *Proc. IEEE*, vol. 60, pp. 389–421, 1972.
27. K. Martha, et al., *Electromagnetic Fields and the Environment (translated from Czech)*, San Francisco Press: San Francisco, 1971.
28. E.G. Kivrak, et al. "Effects of electromagnetic fields exposure on the antioxidant defense system," *Journal of Microscopy and Ultrastructure*, vol. 5, pp. 167–176, 2017.
29. H. Kour, R. K. Jha, "Electromagnetic Radiation Reduction in 5G Networks and Beyond Using Thermal Radiation Mode," *IEEE Transactions on Vehicular Technology*, vol. 69, no 10, pp. 11841-11856, 2020.
30. T. Wu, et al., "The Human body and Millimetre-Wave Wireless Communication Systems: Interactions and Implications," *In Proc. of the IEEE International Conference on Communications*, London, UK, June 08-12, UK, 2015, 15438118.
31. A. Nefzi, "Analysis and dosimetry of the coupling of electromagnetic waves with biological tissues: application to applicator design for biomedical and study of health effects ", Ph.D. Thesis, University of Limoges, 2021.
32. D.N. Erwin, W.D. Hurt, "Assessment of possible hazards associated with applications of mm--wave systems,"Available at: https://apps.dtic.mil/dtic/tr/fulltext/u2/a112014.pdf, Accessed Oct. 20, 2023.
33. O.P. Gandhi, A. Riazi, "Absorption of mm-waves by human beings and its biological implications," *IEEE Trans. Microwave Theory Technology*, vol. 34, pp. 228–235, 1986.
34. P.J. Riu, et al.," A thermal model for human thresholds of microwave-evoked warmth sensations," *Bioelectromagnetic*, vol. 18, pp. 578–583, 1997.
35. H. A. Kues, et al., "Absence of ocular effects after either single or repeated exposure to 10 mW/cm2 from a 60 GHz CW source," *Bioelectromagnetic*, vol. 20, pp. 463–473, 1999.
36. K.L. Ryan, et al., "Radio frequency radiation of m-wave length: potential occupational safety issues relating to surface heating," *Health Phys.*, vol. 78, pp. 170–181, 2020.
37. C.K. Chou, et al., "Radio Frequency Electromagnetic Exposure: Tutorial Review on Experimental Dosimetry," *Bioelectromagnetic*, vol. 17, pp. 195-208, 1996.
38. J. Kaur, S.A. Khan, "Numerical analysis of heat transfer of in multilayered skin tissue exposed to 5G mobile communication frequencies," *Journal of Thermal Engineering*, vol. 7, no 2, pp. 103-116, 2021.
39. R.W.Y. Habash, et al., "Thermal Therapy, Part IV: Electromagnetic and Thermal Dosimetry," *Critical Reviews™ in Biomedical Engineering*, vol. 35, no. (1-2), 123-182, 2007.
40. A. Zamanian, C. Hardiman, "Electromagnetic Radiation and Human Health: A Review of Sources and Effects," *EMR & Human Health*, 2005.
41. L. Hardell, M. Carlberg, M.K. Hansson, M. Eriksson, "Case-control study on the use of mobile and cordless phones and the risk for malignant melanoma in the head and neck region," *Pathophysiology*, vol.18, no 4, 2011.
42. K. Buchner, H. Eger, "Changes of Clinically Important Neurotransmitters under the Influence of Modulated RF Fields A Long-term Study under Real-life Conditions," *Umwelt-Medizin-*

Gesellschaft, Vol. 24(1), 2011.
43. M. Aydin, et al., "Effect of electromagnetic field on the sperm characteristics and histopathological status of testis in rats," M*edycyna Weterynaryjna*, vol. 63, pp. 178–183, 2007.
44. A. Bahaodini, et al., "Low frequency electromagnetic fields long-term exposure effects on testicular histology, sperm quality and testosterone levels of male rats," *Asian Pacific Journal of Reproduction*, vol. 4, pp. 195-200, 2015.
45. J.-G. Yan, "Effects of cellular phone emissions on sperm motility in rats," *Fertility Sterility*, vol. 88, no 4, pp. 957–964, 2007.
46. A.Y. Owda, et al., "The Reflectance of Human Skin in the Millimeter-Wave Band," *Sensors* (Switzerland), vol. 20, no 5, 2020.
47. R. Roelandts, "Cellular phones and the skin," *Dermatology*, vol. 207, no 1, pp. 3-5, 2003.
48. S.C. Verma, et al., "Harmful Effects of 5G Radiations: Review," *International Journal of Industrial Electronics and Electrical Engineering*, vol. 7, no 3, pp. 2347-6982, 2019.
49. M. L. Pall, "*5G : Great risk for EU, US and International Health ! Compelling Evidence for Eight Distinct Types of Great Harm Caused by Electromagnetic Field (EMF) Exposures and the Mechanism that Causes Them*," no. Chapter 2, pp. 1–90, 2018.
50. U. Zaki, et al., "Harmful Effects of 5G On Life with Possible Solution," *Global scientific Journals*, vol. 8, pp. 1-13, 2020.
51. A. Kish, and O. Aerospace, "Fifth Generation Wireless (5G) Effects on Human Biology," no. November, pp. 0–39, 2019.
52. R. N. Kostoff, "Adverse Effects of Wireless Radiation Copyright 2019 RN Kostoff," pp. 1–648, 2019
53. M. Karaboytcheva, "Effects of 5G wireless communication on human health," no. March, 2020.
54. ICNIRP, "ICNIRP guidelines for limiting exposure to time-varying electric and magnetic fields (1Hz – 100 kHz)," *Health Physics*, vol. 99, no 6, pp. 818-836, 2010.
55. ICNIRP, "Guidelines for Limiting Exposure to Electromagnetic Fields (100 kHz to 300 GHz)," *Health Physics*, vol. 118, no 5, pp. 483–524, 2020.
56. W.H. Bailey, et al., "Synopsis of IEEE Std C95.1TM-2019 'IEEE standard for safety levels with respect to human exposure to electric, magnetic, and electromagnetic fields, 0 Hz to 300 GHz," *IEEE Access*, vol. 7, pp. 171346–171356, 2019.
57. A. Hirata, T. Asano, O. Fujiwara, "FDTD analysis of human body-core temperature elevation due to RF far-field energy prescribed in the ICNIRP guidelines," *Physics in Medicine and Biology*, vol. 52, pp. 5013-5023, 2007.
58. ACGIH, "Threshold limit values for chemical substances and physical agents and biological indices," presented at the American Conference of Governmental Industrial Hygienists, Cincinnati, OH, 1996.
59. P. Bernardi, et al., "Specific Absorption Rate and Temperature Elevation in a Subject Exposed in the Far-Field of Radio-Frequency Sources Operating in the 10–900-MHz Range," *IEEE Trans. Biomed. Eng.*, vol. 50, pp. 295-304, 2003.
60. F. Shellock, J. Crues, "Temperature, heart rate, and blood pressure changes associated with clinical imaging at 1.5 T," *Radiology*, vol. 163, no 1, pp. 259-262, 1987.
61. J. Grund, "Planar Multilayer Model of Human Tissue Exposed to a Plane Electromagnetic Wave," *IEEE Journal of electromagnetics, RF, and microwaves in medicine and biology*, vol. 5, pp. 305-312, 2021.
62. P. Parhami, R. Mitra, "Analysis of arbitrarily shaped wire antennas radiating over a loss? Half-space," Electromagnetics Laboratory Report, No. 79-6, US Army Research Office Grant No. DAAg29-77-G-0111, 1979.
63. S. Bourgiotis, et al., "Radiation of a Vertical Dipole over Flat and Lossy Ground using the Spectral Domain Approach: Comparison of Stationary Phase Method Analytical Solution

with Numerical Integration Results," *Electron. Electr. Eng.*, vol. 21, pp. 38–41, 2015.
64. A. Hochman, Y. Leviatan, "A Numerical Methodology for Efficient Evaluation of 2D Sommerfeld Integrals in the Dielectric Half-Space Problem," *IEEE Transactions on Antennas and Propagation*, vol. 58(2), pp. 413-431, 2010.
65. D. Poljak, et al., "On the use of the vertical straight wire model in electromagnetics and related boundary element solution", *Eng. Anal. with Boundary Elements*., vol. 50, pp. 19-28, 2015.
66. X. Li, et al., "Insulates Vertical Antennas Above Ground", *IEEE Transaction on Antennas and Propagation*, vol. 52, pp. 321-324, Jan. 2004.
67. F.M. Pantoja, et al., "Time domain analysis of thin-wire antennas over lossy ground using the reflection-coefficient approximation," *Radio Science*, vol. 44(RS6009), pp. 1-14, 2009.
68. K.A. Norton, "The propagation of radio waves over the surface of the Earth and upper atmosphere — PART 1," *Proceeding of the institute of radio engineers*, vol. 24, no 2, 1936.
69. H. Green, "Derivation of the Norton Surface Wave Using the Compensation Theorem," *IEEE Antennas and Propagation Magazine*, vol. 49, no. 6, pp. 47–57, 2007.
70. J.R. Wait, K.P. Spied, "On the image representation of the quasi-static fields of a line current source above the ground," *Canadian Journal of Physics*, vol. 47, pp. 2731, 1969.
71. O. M. Abo-Seida, "Estimation of the electromagnetic field created at the earth's surface by an overhead line current," *Applied Mathematics and Computation*, vol. 149, pp. 559–565, 2004.
72. M. Galić, et al., "Simple analytical models for the calculation of the electric field radiated by the base station antenna," *Engineering Modelling*, vol. 31, no 1-2, pp. 31-42, 2017.
73. A. Šušnjara, et al., "Electric Field Radiated By a Dipole Antenna Above a Lossy Half Space: Comparison of Plane Wave Approximation with the Modified Image Theory Approach," *In Proc. of the 25th International Conference on Software, Telecommunications and Computer Networks (SoftCOM)*, Split, Croatia, Sept. 21-23, 2017, 1847-358X.
74. L. Li, et al., "Electromagnetic ground-wave propagation over the earth's surface in the transition range," In Proc. of *the International Conference on Mechanical, Electric and Industrial Engineering (MEIE2018)*, Hangzhou, China, May. 26–28, 2018, 1074 012092.
75. R.W.P. King, "Electromagnetic field of a vertical dipole over an imperfectly conducting half-space," *Radio Science*, vol. 25, no 2, pp. 149-160, 1990.
76. R.W.P. King, "Electromagnetic field of a vertical dipole over an imperfectly conducting half-space," *Radio Science*, vol. 25, no 2, pp. 149-160, 1992.
77. R.W.P. King, "The Electromagnetic Field of a Vertical Electric Dipole over the Earth or Sea," *IEEE Transaction on antennas and propagation*, vol. 42, no 3, pp. 382-389, 1994.
78. R.W.P. King, "Electromagnetic field generated in model of human head by simplified telephone transceiver," *Radio Science*, vol. 30, no 1, pp. 267-281, 1995.
79. R.W.P. King, "Electric fields and currents induced in organs of the human body when exposed to ELF and VLF electromagnetic fields," *Radio Science*, vol. 31, no 5, pp. 1153–1167, 1996.
80. R.W.P. King, "Models and Methods for Determining Induced ELF and VLF Electromagnetic Fields in the Human body: A Critical Study," In Proc. of *IEEE 23rd Northeast Bioengineering Conference*, Durham, NH, USA, 21-22 May, 1997, 0-7803-3848-0.
81. R.W.P. King, "Electric Current and Electric Field Induced in the Human body When Exposed to an Incident Electric Field Near the Resonant Frequency," *IEEE Trans. Microwave Theory, and Tech.*, vol. 48, no 9, pp. 1537-1543, 2000.
82. T. Kurniawan, A.W. Wood, "Simplified analysis of near electromagnetic fields from a dipole in lossy dielectric," *IEEE Transactions on Dielectrics and Electrical Insulation*, vol. 17, no 6, pp. 1943 – 1949, 2010.
83. M. Chaaban. et al., "Analytical model for electromagnetic radiation by bare-wire structures," *Progress In Electromagnetics Research*, vol. 45, pp. 395-413, 2012.
84. M.E. Nazari, W. Huang, "Asymptotic solution for the electromagnetic scattering of a vertical

dipole over plasmonic and non-plasmonic half-spaces," *IET Microwave Antennas Propagation*, vol. 15, pp. 704–717, 2021.
85. M. Parise, "On the Electromagnetic Field of an Overhead Line Current Source," *Electronics*, vol. 9, pp. 1-12, 2020.
86. E. Cero Dinarević, et al., "Simple Dosimetry Procedure for Human Exposure to a Field Radiated by a Vertical Dipole Antenna Above Lossy Half Space *Part 2: Calculation of Transmitted Power Density," In Proc. of *the 8th International Conference on Smart and Sustainable Technologies (SpliTech)*, Split / Bol, Croatia, Juny 20-24, 978-953-290-128-3, 2023.
87. E. Cero Dinarević, et al., "Electric Field Radiated By a Vertical Dipole Antenna Above a Lossy Half Space by using Calculated and Assumed Current Distribution," In Proc. of *the 7th International Conference on Smart and Sustainable Technologies (SpliTech)*, Split / Bol, Croatia, July 5-8, 978-1-6654-8828-0, 2022.
88. S. Khalatbari, et al., "Calculating SAR in Two Models of the Human Head Exposed to Mobile Phones Radiations at 900 and 1800 MHz," Progress In Electromagnetics Research Symposium, Cambridge, USA, March 26-29,2006.
89. A. Lojić Kapetanović, and D. Poljak, "Application of Automatic Differentiation in Electromagnetic Dosimetry – Assessment of the Absorbed Power Density in the mmWave Frequency Spectrum," In Proc. Of *6th International Conference on Smart and Sustainable Technologies (SpliTech)*, Bol and Split, Croatia, 2021.
90. D. Poljak, A. Šušnjara, A. Džolić, "Assessment of Transmitted Power Density due to Radiation from Dipole Antenna of Finite Length, Part I: Theoretical background and current distribution," In Proc. Of *6th International Conference on Smart and Sustainable Technologies (SpliTech)*, Bol and Split, Croatia, 2021.
91. C. Durney, H. Nassoudi, M.F. Iskandr, "R*adiofrequency radiation Dosimetry hand book 4 th Ed. USAFSAM Tr-85-73*," USAF schools of aerospace medicine, Brooks Air Force Base, TX 78235, 1986.
92. A. Hirata, et al., "Estimation of Whole-Body Average SAR in Human Models Due to Plane-Wave Exposure at Resonance Frequency," *IEEE Transactions on Electromagnetic Compatibility*, vol. 52(1), pp. 41-48, 2010.
93. P. Stavroulakis, "*Biological Effects of Electromagnetic Fields*," Springer-Verlag Berlin Heidelberg, 2003.
94. T. Iyama, et al., "Novel Specific Absorption Rate (SAR) Measurement Method Using a Flat Solid Phantom," *IEEE Transactions on Electromagnetic Compatibility*, vol. 50, no. 1, pp. 43-51, 2008.
95. D. Poljak, M. Cvetkovic, "*Human Interaction with Electromagnetic Fields: Computational Models in Dosimetry 1st Edition, Kindle Edition*," Academic Press; 1st edition, 2019.
96. M.O. Khaled, F.A.A.Z. Dalia, "The SAR values predicted by "RDTD" using a mouse body model," *The Egyptian Society of Experimental Biology*, vol. 3, pp-333-340, 2007.
97. B. Durney, "Electromagnetic dosimetry for models of humans and animals: A review of theoretical and numerical techniques," *In Proceedings of the IEEE*, vol. 68, pp. 33-40, 1980.
98. L. Tognolatti, et al., "An Efficient Computational Technique for the Electromagnetic Scattering by Prolate Spheroids," *Mathematics*, vol. 10, 1761-1775.
99. N. Kuster, et al., "Energy absorption mechanism by biological bodies in the near field of dipole antennas above 300 MHz," *IEEE Transactions on Vehicular Technology*, vol. 41, no 1, pp. 17–23, 1992.
100. D. Poljak, Y.F. Rashed, "The boundary element modelling of the human body exposed to the ELF electromagnetic fields," *Engineering Analysis with Boundary Elements*, vol. 26, pp. 871–875, 2002.
101. D. Poljak, N. Kovač, "A Simplified Electromagnetic-thermal Analysis of Human Exposure to Radiation from Base Station Antennas, *Automatika*, vol. 45, no 1–2, pp. 11–17,

2004.
102. B., Kibret, et al., "Human Body as Antenna and Its Effect on Human Body Communications," *Progress In Electromagnetics Research*, vol. 148, pp.193-207, 2014.
103. A. Laissaoui, B. Nekhoul, S. Mezoued & D. Poljak, "Assessment of the human exposure to transient and time-harmonic fields using the enhanced transmission line theory approach," *Automatika*, vol. 58(4), pp. 355-362, 2017.
104. V. Roje, "Safety aspects of the GSM base station radiation concerning human health," In Proc. of *IEEE International Symposium on Electromagnetic Compatibility*, 2003. EMC '03, May 11-16, Istanbul, Turkey, 2003.
105. K. Fukunaga, S. Watanabe, Y. Yamanaka, "Dielectric properties of tissue-equivalent liquids and their effects on specific absorption rate," *IEEE Trans Electromagnetic Compatibility*, vol. 46, pp. 126-129, 2004.
106. R.G. Olsen, "Preliminary studies: far-field microwave dosimetric measurements of a full-scale model of man," *J Microw Power*, vol. 14, no 4, pp. 383-388, 1979.
107. R.G. Olsen, T.A. Griner, "Outdoor measurement of SAR in a full-sized human model exposed to 29.9 MHz in the near field," *Bioelectromagnetics*, vol. 10, no 2, pp. 161-171, 1989.
108. H. Yamaguchi, et al., "Three-dimensional digital representation of human phantom for organ dose calculation," In Proc. Of *XIV International Conference on Medicul und Biological Engineering and Vi Iinternational Conference on Medical Physics*, 6 and 1 July, 1985, Espoo, Finland
109. R. McIntosh, V. Anderson, "SAR Versus Sinc: What Is the Appropriate RF Exposure Metric in theRange1-10 GHz? Part II: Using Complex Human Body Models," *Bioelectromagnetics*, vol. 31, pp. 467-478, 2010.
110. P. Dimbylow, "Resonance voxel of whole-body averaged specific energy absorption rate (SAR) in the female voxel model, NAOMI," *Phys Med Biol*, vol. 50, no 17, pp. 4053-4063, 2005.
111. M. Lazebnik, et al., "Tissue-mimicking phantom materials for narrowband and ultrawideband microwave applications," Phys Med Biol, vol. 50, no 18, pp. 4245-4258, 2005.
112. I.J. Youngs, et al., "Design of solid broadband human tissue simulant materials," *IEEE Proc Sci Meas Tech*, vol. 149, no 6, pp. 323-328, 2002.
113. P.J. Dimbylow, "FDTD calculations of the whole-body averaged SAR in an anatomically realistic voxel model of the human body from 1 MHz to 1 GHz," *Phys. Med. Biol*., vol. 42, no 3, pp. 479-490, 1997.
114. T.W. Dawson, K. Caputa, M.A. Stuchly, "A comparison of 60 Hz uniform magnetic and electric induction in the human body," *Phys. Med. Biol.*, vol. 42, no 12, pp. 2319-2329, 1997.
115. C.M. Furse, O.P. Gandhi, "Calculation of electric fields and currents induced in in a mm-resolution human model at 60 Hz using the FDTD method," *Bioelectromagnetics*, vol. 19, no 5, pp. 293-299, 1998.
116. C. Lee, et al., "Whole-body voxel phantoms of paediatric patients—UF Series B.," *Phys. Med. Biol.*, vol. 51, no 18, pp. 4649- 4661, 2006.
117. P.A. Mason, et al., "*Recent advancements in dosimetry measurements and modeling*". In: Klauenberg, B.J., Miclavcic, D., eds. Radio frequency radiation dosimetry and its relationship to the biological effects of electromagnetic fields. Dordrecht, Kluwer Academic Publishers, pp. 141-155, 2000.
118. T. Nagaoka, et al., "Development of realistic high-resolution whole-body voxel models of Japanese adult males and females of average height and weight, and application of models to radio-frequency electromagnetic field dosimetry," *Phys Med Biol*, vol. 49, no 1, pp.1-15, 2004.
119. I.G. Zubal, C.R. Harrell, et al., "Computerized three-dimensional segmented human

anatomy," *Med. Phys*., vol. 21, pp. 299-302, 1994.
120. ICRP, "*Report of the Task Group on Reference Man*", ICRP Publication 23. Pergamon Press, Oxford, 1975.
121. ICRP, "Basic Anatomical and Physiological Data for Use in Radiological Protection Reference Values", ICRP Publication 89. Ann. ICRP, Vol. 32 (3-4), 2002.
122. M. Zankl, et al., "Computational phantoms, ICRP/ICRU, and further developments," *Ann. ICRP*., vol. 47, no 3-4, pp. 35-44, 2018.
123. A. Christ, et al., "The Virtual Family--development of surface-based anatomical models of two adults and 880 two children for dosimetric simulations," *Phys. Med. Biol.*, vol. 55(2), pp. 23-38, 2010.
124. C. Lee, et al., "Whole-body voxel phantoms of paediatric patients—UF Series B.," *Phys. Med. Biol.*, vol. 51, no 18, pp. 4649- 4661, 2006.
125. Stuchly, M.A. et al.: RF energy deposition in a heterogeneous model of man: near-field exposures, *IEEE Trans. Biomed. Eng.*, Vol. 34(12), pp. 944-950, 1987.
126. O.P. Gandi, et al., "Millimeter-resolution MRI-based models of the Human Body for Electromagnetic Dosimetry from ELF to Microwave Frequencies, Voxel Phantom Development ", In Proc. Of *the International Workshop At: National Radiological Protection Board (NRPB),* Project: Implantable Antennas (medical, geophysical, plasma applications), 1995.
127. R.S. Damor, S., Kumar, A.K. Shukla, "Solution of fractional bioheat equation in terms of Fox's H-function," *SpringerPlus*, vol. 5, pp. 111-121, 2016.
128. T.C. Shih, et al., "Analytical analysis of the Pennes bioheat transfer equation with sinusoidal heat flux condition on skin surface," *Med. Eng. Phys*., vol. 29, pp. 946–953, 2007.
129. H.H. Pennes, "Analysis of tissue and Arterial Blood Temperatures in the Resting Human Forearm," *Journal of Applied Physiology*, vol. 1, pp. 93-122, 1948.
130. N. Kizilova, A. Korobov, "Bioheat equation with Fourier and non-Fourier heat transport laws: applicability to heat transfer in human tissues," *Journal of Thermal Engineering*, vol. 5, no 6, pp. 149-161, 2019.
131. J. Tao, et al., "A Combination of Laplace Transform and Meshless Method for Analysing Thermal Behaviour of Skin Tissues," *Universal Journal of Mechanical Engineering*, vol. 1, no 2, pp. 32-42, 2013.
132. D. Aatef, et al., "Theoretical analysis of thermal damages in skin tissue induced by intense moving heat source," *International Journal of Heat and Mass Transfer*, vol. 124, pp. 1011-1014, 2018.
133. A. Lakhssassi, et al., "Modifed pennes' equation modelling bio-heat transfer in living tissues: analytical and numerical analysis," *Natural Science*, vol. 2, pp. 1-12, 2010.
134. J. Hand, E. Thomas, M. Rutherford and J. Hajnal, "Prediction of Specific Absorption Rate in Mother and Fetus Associated With MRI Examinations During Pregnancy," *Magn. Reson. Med.*, pp. 883-893, 2006.
135. R. Roemer and T. Cetas, "Applications of Bioheat Transfer Simulations in Hyperthermia," *Cancer Res.*, vol. 44, pp. 4788-4798, 1984.
136. D.W. Hahn, M.N. Ozisik, *Heat Conduction*, 3th Edition, New Jersey: John Wiley & Sons, Inc., 2012. Accessed: August 18, 2023.
137. D. Fiala, et al., "A computer model of human thermoregulation for a wide range of environmental conditions: the passive system," *J. Appl. Physiol.*, vol. 87(5), pp.1957- 2022, 1999.
138. Z.S. Deng, J. Liu, "Monte carlo method to solve multidimensional bioheat transfer problem," *Numer. Heat Transfer*, vol. 42, pp. 543–567, 2002.
139. J.W. Durkee, P.P. Antich, „Exact-solution to the multiregion time dependent bioheat equation with transient heat-sources and boundary-conditions," *Phys. Med. Biol*., vol. 36, pp. 345-368, 1991.

140. J.W. Durkee, P.P. Antich, C.E. Lee, „Exact-solutions to the multiregion time-dependent bioheat equation 1. Solution development,“ *Phys. Med. Biol.*, vol. 35, pp. 847-867, 1990.
141. G. Shen, G., S. Xie, “Theoretical Analysis and Numerical Simulation of Temperature Distribution for Laser-Irradiated Skin Tissue,” *Journal of Fujian Teachers University* (Natural Science), vol.18(4), pp. 26–29, 2002.
142. R. Cai, “Analytical Solution of Unsteady One-Dimensional Bioheat Transfer Equation,” *Chin. Sci. Bull.*, vol. 40(19), pp. 1663-1665, 1995.
143. J. Steketee, and M.J. Van Der Hoek, “Thermal Recovery of the Skin After Cooling,” Phys. Med. Biol., vol. 24(3), pp. 583–592, 1979.
144. W.L. Nyborg, “Solutions of the Bio-Heat Transfer Equation,” *Phys. Med. Biol.*, vol. 33(7), pp. 785–792, 1988.
145. H. Li, et al., “Heat Transfer Analysis on Laser-Tissue Thermal Interaction Using Heterogeneous Model,” *Chin. J. Lasers*, vol A29(5), pp. 465–470, 2002.
146. D.A. Timoshenko, et al., “Mathematical Simulation of Heat-Induced Effects on Human Skin Surface,” *Biomed. Eng. Online*, 36(1), pp. 19–22, 2002.
147. S. Özen, et al., “Heat Effect Analysis of Microwave Exposed Skin by Using a Multilayer Human Skin Model,” Bioeffects of EMFS, Second International Workshop, Rhobes, Greece, 2002.
148. T. Dai, “A Theoretical Investigation of Human Skin Thermal Response to Near-Infrared Laser Irradiation,” In Proc. of the *International Society for Optical Engineering*, Bellingham, WA, pp. 7–12, 2004.
149. Ng, E.Y.K., and L.T. Chua, “Quick Numerical Assessment of Skin Burn Injury With Spreadsheet in PC,” *International Journal of Mechanics Medical Biology*, vol. 1(1) pp. 1–10, 2001.
150. T.R. Gowrishankar, et al., “Transport Lattice Models of Heat Transport in Skin With Spatially Heterogeneous, Temperature-Dependent Perfusion,” *Biomed. Eng. Online*, vol. 3(1/42), pp. 1–17, 2004.
151. S. Jiang, et al., “Analysis of Heat Transfer and Prediction of Skin Burn Subjected to a Hot Water Film,” *Space Med. Med. Eng. (Beijing)*, vol. 16(6), pp. 400–404, 2003.
152. S.C. Jiang, et al. “Analysis of Heat Transfer in Skin Tissues Subjected to Hot Water,” *Space Med. Med. Eng. (Beijing)*, vol. 16(1), pp. 44–47, 2003.
153. N. Ma, et al. “Analysis of Non-Flourier Effect and Laser-Induced Thermal Damage of Laser-Irradiated Layered Human Skin Tissue,” *Space Med. Med. Eng. (Beijing)*, 16(2), pp. 133–137, 2003.
154. T.N. Andersen, et al., “Determination of the Temperature Distribution in Skin Using a Finite Element Model,” In Proc. of the *Laser-Tissue Interaction XI: Photochemical, Photothermal, and Photomechanical*, SPIE, San Jose, CA, pp. 54–65, 2000.
155. F. Gustrau, and A. Bahr, “W-Band Investigation of Material Parameters, SAR Distribution, and Thermal Response in Human Tissue,” *IEEE Trans. Microwave Theory Tech.*, vol. 50(10), pp. 2393–2400, 2002.
156. Dodig, D. Poljak and A. Peratta, "Hybrid BEM/FEM edge element computation of the thermal rise in the 3D model of the human eye induced by high frequency EM waves," SoftCOM 2012, In Proc. of the *20th International Conference on Software, Telecommunications and Computer Networks*, Split, Croatia, 2012, pp. 1-5.
157. H.M. Patil, R. Maniyeri, “Finite difference method based analysis of bio-heat transfer in human breast cyst,” *Thermal Science and Engineering Progress*, vol. 10, pp. 42-47, 2019.
158. R.E. Chatterjee, “Finite element thermal modeling of the human body under hyperthermia treatment for cancer,” *International Journal of Computer Applications in Technology*, vol. 1, pp. 151-159, 1994.
159. J. Drozdek, E. Majchrzak, “Numerical solution of bioheat transfer equation by means

of the dual reciprocity BEM," *Scientific Research of the Institute of Mathematics and Computer Science,* vol. 6(1), pp. 47-56, 2007.
160. Z.-S. Deng, J. Liu, "Monte Carlo Simulation of the Effects of Large Blood Vessels During Hyperthermia," in Proc Of Lecture Notes in Computer Science book series (LNCS, vol. 3314), 2004.
161. H. Bansu, S. Kumar, "Meshless Method for Numerical Solution of Fractional Pennes Bioheat Equation," in Proc Of IFMBE Proceedings book series (IFMBE,volume 79), Jan. 2012.
162. J. Tao, et al., "A Combination of Laplace Transform and Meshless Method for Analysing Thermal Behaviour of Skin Tissues," *Universal Journal of Mechanical Engineering,* vol. 1, no 2, pp. 32-42, 2013.
163. K.A. Abro, et al., "An analytic study of bioheat transfer Pennes model via modern non-integers differential techniques," *Eur. Phys. J. Plus,* vol. 136, pp. 1144-1155, 2021.
164. A.T. Cole, R.O. Olayiwola, "Variational Iteration Method for Solving Partial Differential Equation Arising from Modeling Heat Transfer in Human Tooth," *International Journal of Sciences: Basic and Applied Research (IJSBAR),* vol. 46(2), pp. 1-7, 2019.
165. R. Kumar, et al., "Analytical solution of bioheat transfer equation with variable thermal conductivity in skin," *International Journal Of Engineering Research And Development,* vol. 14, pp.11-17, 2017.
166. S. Hossain, "One-dimensional Steady-state Analysis of Bioheat Transfer Equation: Tumour Parameters Assessment for Medical Diagnosis Application," Department of Electrical and Computer Engineering, Ryerson University Toronto, ON, M5B 2K3, Canada, 2013.
167. Z.-S. Deng, J. Liu, "Analytical Solutions to 3-D Bioheat Transfer Problems with or without Phase Change," Heat Transfer Phenomena and Applications, 2012.

Abbreviation list

ANSI	American National Standards Institute
BEM	Boundary Element Method
BC	Boundary Condition
CAD	Computer Aided Design
CDMA	Code Division Multiple Access
CT	Computer Tomography
D2D	Device-to-Device
DNA	Deoxyribonucleic acid
DRBEM	Dual Reciprocity BEM
EDGE	Enhanced Data rates for GSM Evolution
EFIE	Electric Field Integral Equation
ELF	Extreme LF
EM	Electromagnetic
eMB	enhanced Mobile Broadband
EMF	EM field
ES	Electromagnetic hypersensitivity
FAX	Female Adult voXel
FDM	Finite Difference Method
FDMA	Frequency Division Multiple Access
FDTDM	Finite-difference time-domain method
FEM	Finite Element Method
GPRS	General Packet Radio Service
GSM	Global System for Mobile
HF	High Frequency
HSDPA	High-Speed Downlink Packet Access
HSPA	High Speed Packet Access
HSUPA	High-Speed Uplink Packet Access
ICNIRP	International Commission on Non-Ionizing Radiation Protection
IMR	Intensity Modulated Radiotherapy
IMT	International Mobile Telecommunications
IP	Internet Protocol
ITU	International Telecommunication Union
LF	Low Frequency
LTE	Long-Term Evolution
MAX	Male Adult voXel
MCM	Monte Carlo Method
MF	Medium Frequency
MI	Medical Imagery
MIT	Modified Image Theory
MPBH	Method based on modified PBE
mMTC	Massive Machine Type Communications
mm-wave	Millimeter wave
MRI	Magnetic Resonance Imaging
MSEETBM	Models for Simulation of Electromagnetic, Elastomechanic and Thermic Behavior of Man

NCRPM	National Council on Radiation Protection and Measurements
NMAE	Normalized Maximum Absolute Error
NR	New Radio
NRMSE	Normalized Root-Mean-Square Error
OFDMA	Orthogonal Frequency Division Multiple Access
PBE	Penne's Bioheat Equitation
PDE	Partial Differential Equation
PLC	Power Line Communication
PSTN	Packet Switch Telephone Network
RAT	Radio Access Technologies
RF	Radio Frequency
RVM	Reduced Visible Human
SAR	Specific Absorption Rate
SCFDMA	Single- carrier FDMA
SEA	Specific energy Absorption
SPM	Saddle Point Method
SoV	Separation of Variables
TDMA	Time Division Multiple Access
UHF	Ultra HF
UMTS	Universal Mobile Telecommunication System
uRLL	ultra-Reliable and Low Latency
VHF	Very HF
VIM	Variational Iteration Method
VIPMAN	Visible Photography-Man
VLF	Very LF
WCDMA	Wideband Code Division Multiple Access
WIMA	Worldwide Interoperability for Microwave Access
WWW	World Wide Web
3DBF	Three-dimensional beamforming
3GPP	3rd Generation Partnership Project

Abstract

Due to the increasing use of mobile terminals, the importance of accurate evaluation of the mechanisms of interaction of electromagnetic waves with the human body has increased significantly. On the other hand, rapid technological development and the widespread presence of smart environments has led to the need for rapid implementation of systems, which further means rapid assessments of the impact of these systems on the human body. Computer methods for analyzing problems in electromagnetics generally fall into one of three categories, analytical techniques, numerical techniques, and expert systems [1]. Analytical techniques make simplifying assumptions about the geometry of a problem and EM field equations are solved directly. Numerical techniques attempt to solve fundamental field equations directly, subject to the boundary constraints posed by the geometry. Expert systems do not actually calculate the field directly, but instead estimate values for the parameters of interest based on a rules database.

All effects (thermal and other) of the action of electromagnetic fields (EMF) must be well researched or described, regardless of whether we want to protect ourselves from the potential harmful effects of EMF or we want to take advantage of their potential positive effects. In the past few decades there has been a lot of effort to cope with aforementioned challenges keeping in mind computer resources and minimum accuracy level. Contrary to numerical approaches the analytical based ones aim to represent the radiated electric field in the form which can be solved analytical. Keeping what we said beforehand in mind, our goal is two-fold. At the beginning we highlighted the importance of the topic, so the Chapter 2 introduces some basic concepts of evolution of mobile network technologies (2G – 5G) and the main difference between different generations of mobile network.

In chapter 3 the interaction between human being and EMF is described. The basic potential risk associated with excessive exposure to EM radiation and some guidance for human health protection from the harmful effects of EM waves are given. The recommendations for exposure limitation are given in different frequency ranges, highlighting High Frequency (HF) range.

The second goal is to outline some of the commonly used analytical methods in electromagnetic-thermal dosimetry along with the advantages and limitations. Incident dosimetry concept are described in chapter 4. Different methods for dosimetry are explained and then short literature review of analytical approaches is given with the aim to emphasis possible simplification and advantages offer by these approaches to EM dosimetry. After

detailed explanation of analytical methods, simple scenario with vertical Hertzian dipole antenna in far field is observed and corresponding field equations are presented.

After incident dosimetry concept, basic concepts of internal EM dosimetry are given in chapter 5. Since analytical methods are used when a problem requires an accurate solution, they are mostly related to canonical problems. Further on, comparation between canonical models and complex voxel models are given, followed by short description of basic canonical models mentioned in analyzed literature.

In chapter 6, thermal dosimetry concepts are explained followed by analytical approaches to solution of Penne's bioheat equation, as the most used equation for energy balance between conductive heat transfer per tissue volume unit, heat losses due to perfusion, metabolism and energy absorption due to radiation.

Finally, chapter 7 gives some conclusion remarks, pointing the problem towards the need for the spectrum of analytical methods that are accurate enough, but simple enough, to be used in the upcoming 5G systems and broader.

.

Sažetak

Zbog sve veće upotrebe mobilnih terminala značajno je porasla važnost točne procjene mehanizama interakcije EM valova s ljudskim tijelom. S druge strane, brzi tehnološki razvoj i raširenost pametnih okruženja doveli su do potrebe za brzom implementacijom sustava, što dalje znači brze procjene utjecaja tih sustava na ljudski organizam. Računalne metode za analizu problema u elektromagnetici općenito spadaju u jednu od tri kategorije, analitičke tehnike, numeričke tehnike i ekspertni sustavi [1]. Analitičke tehnike donose pojednostavljene pretpostavke o geometriji problema, a jednadžbe EM polja rješavaju se izravno. Numeričke tehnike pokušavaju izravno riješiti temeljne jednadžbe polja, podložne graničnim ograničenjima postavljenim geometrijom. Ekspertni sustavi zapravo ne izračunavaju polje izravno, već umjesto toga procjenjuju vrijednosti za parametre od interesa na temelju baze podataka pravila.

Svi učinci (toplinski i drugi) djelovanja EMFs moraju biti dobro istraženi ili opisani, bez obzira na to želimo li se zaštititi od potencijalnih štetnih učinaka EM polja ili želimo iskoristiti njihove potencijalne pozitivne učinke. U posljednjih nekoliko desetljeća uloženo je mnogo truda da se nosi s gore navedenim izazovima imajući na umu računalne resurse i minimalnu razinu točnosti. Nasuprot numeričkim pristupima, analitički zasnovani pristupi imaju za cilj prikazati zračeno električno polje u obliku koji se može analitički riješiti. Imajući na umu ono što smo prethodno rekli, naš cilj je dvostruk. Na početku smo istaknuli važnost teme, stoga 2. poglavlje uvodi neke osnovne koncepte evolucije tehnologija mobilnih mreža (2G – 5G) i glavne razlike između različitih generacija mobilnih mreža.

U poglavlju 3 opisana je interakcija između čovjeka i EM polja. Dat je osnovni potencijalni rizik povezan s prekomjernom izloženošću EM zračenju i neke smjernice za zaštitu zdravlja ljudi od štetnog djelovanja EM valova. Preporuke za ograničenje izloženosti dane su u različitim frekvencijskim rasponima, ističući HF raspon.

Drugi cilj je prikazati neke od često korištenih analitičkih metoda u elektromagnetsko-termalnoj dozimetriji zajedno s prednostima i ograničenjima. Koncept incidentne dozimetrije opisan je u poglavlju 4. Objašnjene su različite metode dozimetrije, a zatim je dan kratak pregled literature o analitičkim pristupima s ciljem naglašavanja mogućeg pojednostavljenja i prednosti koje ti pristupi EM dozimetriji nude. Nakon detaljnog objašnjenja analitičkih metoda, promatran je

jednostavan scenarij s vertikalnom Hertzovom dipolnom antenom u dalekom polju i prikazane su odgovarajuće jednadžbe polja.

Nakon koncepta incidentne dozimetrije, osnovni koncepti interne EM dozimetrije dani su u poglavlju 5. Budući da se analitičke metode koriste kada problem zahtijeva točno rješenje, one se uglavnom odnose na kanonske probleme. Nadalje je dana usporedba između kanoničkih modela i složenih voxel modela, nakon čega slijedi kratak opis osnovnih kanoničkih modela koji se spominju u analiziranoj literaturi.

U poglavlju 6 objašnjeni su koncepti toplinske dozimetrije, a zatim analitički pristupi rješavanju Penneove jednadžbe biotopline, kao najčešće korištene jednadžbe za ravnotežu energije između konduktivnog prijenosa topline po jedinici volumena tkiva, gubitaka topline zbog perfuzije, metabolizma i apsorpcije energije zbog zračenja .

Konačno, poglavlje 7 daje neke zaključke, ukazujući na problem prema potrebi za spektrom analitičkih metoda koje su dovoljno precizne, ali dovoljno jednostavne, da se koriste u nadolazećim 5G sustavima i šire.